Supplementary Materials for

Reversible centriole depletion with an inhibitor of Polo-like kinase 4

Yao Liang Wong, John V. Anzola, Robert L. Davis, Michelle Yoon, Amir Motamedi, Ashley Kroll, Chanmee P. Seo, Judy E. Hsia, Sun K. Kim, Jennifer W. Mitchell, Brian J. Mitchell, Arshad Desai, Timothy C. Gahman, Andrew K. Shiau,* Karen Oegema*

*Corresponding author. E-mail: koegema@ucsd.edu(K.O.); ashiau@ucsd.edu (A.K.S.)

Published 30 April 2015 on *Science* Express
DOI: 10.1126/science.aaa5111

This PDF file includes

Other Supplementary Material for this manuscript includes the following:
(available at www.sciencemag.org/cgi/content/full/science.aaa5111/DC1)

Table S3. DiscoveRx KINOMEscan profiling of centrinone (100 nM) and centrinone-B (300 nM) against 442 human kinases. (as an Excel table)

Materials and Methods

Centrinones

Centrinone (LCR-263) and centrinone-B (LCR-323) were synthesized by Sundia Meditech, Shanghai, China.

Centrinone (LCR-263)

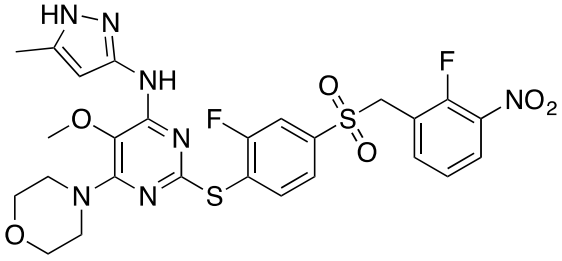

2-((2-fluoro-4-((2-fluoro-3-nitrobenzyl)sulfonyl)phenyl)thio)-5-methoxy-*N*-(5-methyl-1*H*-pyrazol-3-yl)-6-morpholinopyrimidin-4-amine was prepared by Sundia Meditech, Shanghai, China. ^{1}H NMR (400 MHz , CD_3OD): δ 8.11 (t, 1 H), 7.88 (t, 1 H), 7.67-7.74 (m, 2 H), 7.61 (d, 1 H), 7.39-7.43 (t, 1 H), 5.99 (s, 1 H), 4.82 (s, 2 H), 3.63-3.66 (m, 7 H),.3.51-3.53 (m, 4 H), 3.32 (s, 3 H). ^{13}C NMR (100 MHz, DMSO-*d6*): δ 168.12, 165.61, 165.00, 159.54, 157.93, 150.85, 146.05, 145.93, 144.29, 143.24, 142.55, 132.20, 130.69, 130.13, 129.70, 127.90, 124.13, 120.93, 100.45, 71.33, 64.03, 59.32, 51.39, 16.23. HRMS(ESI) *m/z* for $C_{26}H_{26}F_2N_7O_6S_2$ $[M+1]^+$ calculated 634.1354, found 634.1367.

Centrinone-B (LCR-323)

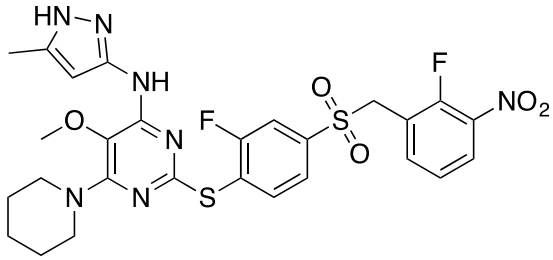

2-((2-fluoro-4-((2-fluoro-3-nitrobenzyl)sulfonyl)phenyl)thio)-5-methoxy-*N*-(5-methyl-1*H*-pyrazol-3-yl)-6-(piperidin-1-yl)pyrimidin-4-amine was prepared by Sundia Meditech, Shanghai, China. ^{1} H NMR (400 MHz, CD_3OD): δ 8.07-8.12 (m, 1 H), 7.88 (t, 1 H), 7.60-7.65 (m, 2 H), 7.36 (t, 1 H), 5.68 (s, 1 H), 4.79 (s, 2 H), 3.62 (s, 3 H), 3.51-3.53 (m, 4 H), 2.14 (s, 3 H), 1.56-1.64 (m, 6 H). ^{13} C NMR (100 MHz, DMSO-*d6*): δ 162.88, 160.38, 159.52, 154.21, 152.64, 145.87, 140.63, 140.45, 139.03, 138.02, 137.30, 126.95, 125.50, 124.90, 124.38, 122.06, 118.89, 115.55, 95.10, 58.60, 54.01, 46.49, 25.49, 24.15, 11.02. HRMS(ESI) *m/z* for $C_{27}H_{28}F_2N_7O_5S_2$ $[M+1]^+$ calculated 632.1561, found 632.1548.

Chemical inhibitors

CFI-400945 (0.01-0.1 μM) and R7112 (0.3 μM) were synthesized by Sundia Meditech.

The following chemical inhibitors were purchased from commercial sources, with their working concentrations indicated in parentheses: VX-680 (1 μM; Selleck Chem); nocodazole

(0.08-16 μM; Sigma-Aldrich); doxorubicin (0.5-2 μM; Sigma-Aldrich); SB203580 (10 μM; LC Labs); KU-60019 (2 μM; Selleck Chem); VE-821 (2 μM; Selleck Chem); MK-8776 (0.5 μM; Selleck Chem); NU7441 (1 μM; Tocris); AZ3146 (2 μM; Tocris); NMS-P715 (1 μM; EMD Millipore).

Antibodies

Antibodies against Cep192, SAS-6 and Plk4 were generated by injecting GST fusions of Cep192 aa 1-211, SAS-6 aa 501-657 and Plk4 aa 814-970, respectively, into rabbits. Antibodies were affinity-purified using standard procedures (*36*). Cep192 and SAS-6 antibodies were used at 0.5 μg/ml. The Plk4 antibody was used at 1 μg/ml.

The following antibodies were purchased from commercial sources, with their working concentrations indicated in parentheses: GTU-88 (anti-γ-tubulin; 1:1000; Sigma-Aldrich); anti-centrin-1 (1μg/ml; Abcam); anti-pericentrin (1μg/ml; Abcam); anti-CPAP (1:400; ProteinTech); anti-IFT-88 (1:100; ProteinTech); anti-GM130 (1μg/ml; Abcam); anti-GFP (0.4 μg/ml; Roche); anti-LATS2 (1 μg/ml; Abcam); anti-p-LATS2(Ser83) (1:500; Cyclex); anti-p-H3(Ser10) (1:100; Cell Signaling); Alexa488-conjugated anti-p-H3(Ser10) (1:200; Cell Signaling); anti-YAP (0.5 μg/ml; Santa Cruz); anti-p-YAP(Ser127) (1:1000; Cell Signaling); YL1/2 (anti-tubulin; 1:500; Abcam); anti-p-p38(Thr180/Tyr182) (1:1000; Cell Signaling); anti-MAPKAPK-2 (1:1000; Cell Signaling); anti-p-MAPKAPK-2(Thr334) (1:1000; Cell Signaling); anti-p53 (1:100; Calbiochem); anti-p-p53(Ser9) (1:1000; Cell Signaling); anti-p-p53(Ser15) (1:250; MBL); anti-p-p53(Ser20) (1:1000; Abcam); anti-p-p53(Ser33) (1:1000; Cell Signaling); anti-p-p53(Ser37) (1:1000; Cell Signaling); anti-p-p53(Ser315) (1:1000; Cell Signaling); anti-p-p53(Ser392) (1:1000; Cell Signaling); anti-acetyl-p53(Lys382) (1:1000; Cell Signaling); anti-p21 (1:1000; Cell Signaling); anti-MDM2 (1:1000; Millipore); anti-γ-H2A.X (1μg/ml; Abcam); DM1A (anti-α-tubulin; 1:1000; Sigma-Aldrich); anti-GAPDH (1:1000; Cell Signaling). Secondary antibodies were purchased from Jackson Immunoresearch.

Kinase assays

All kinase assays were performed in Corning #3674 white 384-well plates. Plk4 assays used equal volumes of: (1) purified 6xHis-tagged human Plk4 kinase domain (aa 2-275) (expressed in *E. coli* and purified via Ni-NTA affinity chromatography) in 20 mM Tris pH 7.5, 100 mM NaCl, 10% glycerol, 1 mM DTT; (2) 2X reaction buffer consisting of 50 mM HEPES pH 8.5, 20 mM $MgCl_2$, 1 mM DTT, 0.2 mg/ml BSA, 16 μM ATP, and 200 μM A-A11 substrate (amino acid sequence: TPSDSLIYDDGLS; *17*). The Plk4 concentration in the final reaction was 2.5-10 nM with a final pH of 8.0. Inhibitors arrayed in dose response were added from DMSO stocks using a V&P 384-pintool head mounted on a Beckman Multimek chassis. Reactions were allowed to proceed for 4-16 hours at 25°C. Detection was performed using ADP-Glo reagent (Promega), following manufacturer's instructions. Luminescence was measured on an Infinite M1000 plate reader (Tecan). Data were fit using Prism (GraphPad) and K_is were calculated from IC_{50} data using the Cheng and Prusoff equation (*37*) or the Copeland formalism for tight-binding inhibitors (*38*).

Aurora A assays used 1 nM purified human Aurora A (Millipore) in 25 mM Tris pH 7.5, 75 mM NaCl, 10 mM $MgCl_2$, 135 mM Sucrose, 0.5 mM DTT, 0.1 mg/ml BSA, 0.015% Brij 35 + 35 μM ATP + 400 μM Kemptide substrate (amino acid sequence: LRRASLG) + inhibitors arrayed in dose response (added as described above). Reactions were incubated for 1 hour at 25°C. Detection, measurement and data analysis were performed as described above.

Aurora B and other radiometric kinase assays were performed by Reaction Biology (Malvern, PA). Kinome profiling of centrinone and centrinone-B was performed by DiscoveRx (San Diego, CA).

Crystal structure of centrinone-bound Plk4

Human Plk4 (aa 2-275) was cloned into pET42 with an N-terminal GST-6xHis tag. The fusion protein was co-expressed with λ-phosphatase (cloned into pCDF-Duet1 (Novagen)) in *E. coli* BL21 Rosetta2(DE3) cells (Novagen) and purified by affinity chromatography with Ni-NTA Superflow resin (Qiagen) followed by glutathione Sepharose 4 Fast Flow (GE) using standard methods. The tag was cleaved with Turbo3C protease (ETON), and removed using glutathione Sepharose. The untagged protein was further purified by size-exclusion chromatography on a GE Superdex 75 16/600 column. The final eluate (in 20 mM Tris pH 7.5, 100 mM NaCl, 0.5 mM TCEP) was incubated with 100 μM centrinone overnight on ice, then concentrated to ~8 mg/mL using Amicon Ultra 10K MWCO concentrators (Millipore).

Plk4(2-275) + centrinone was crystallized by sitting drop vapor diffusion using a reservoir buffer consisting of 0.1 M HEPES pH 7.5, 0.2 M $MgCl_2$, 30% PEG-400 at 24°C. 0.2 μL protein solution was mixed with 0.1 μL reservoir buffer using a Mosquito pipettor (TTP Labtech) and sealed in a chamber containing 70 μL of reservoir solution. After 8 months, a single cubic crystal (~30 μm edge) was transferred to a cryoprotectant containing 0.1 M HEPES pH 7.5, 0.2 M $MgCl_2$, 32.5% PEG 400, 100 μM centrinone, and flash-frozen in liquid nitrogen.

X-ray diffraction data were measured at the NE-CAT beamline 24-ID-E at the Advanced Photon Source at Argonne National Laboratory and processed with XDS (*39*) and AIMLESS from the CCP4 suite (*40*). The structure was determined by molecular replacement using PHASER (*41*) and sequential searches with the large and then the small lobe of the kinase domain model of the AMP-PNP complex (PDB: 3COK). Refinement was performed using PHENIX (*42*) interspersed with iterative cycles of rebuilding using Moloc (*43*). Figures were made using PyMol (Schrödinger).

Cell lines

Primary cells and cell lines were obtained from the ATCC, with the exception of N1E-115-1 (Sigma-Aldrich), Tet-On 3G NIH/3T3 (Clontech), DLD-1 Plk4-YFP (gift from A. Holland and D. Cleveland) and RPE1 Fucci YAP (WT and S5A; gifts from N. Ganem and D. Pellman). Cells were generally maintained in ATCC-recommended complete growth media + 100 U/mL penicillin + 100 μg/mL streptomycin. Compounds were added to and maintained in complete growth medium unless otherwise specified.

For generation of Plk4-GFP inducible NIH/3T3 cells, a mouse Plk4 cDNA C-terminally fused to eGFP was cloned into the lentiviral vector pLVX-TRE3G (Clontech). The G95L point mutation was generated by Quikchange mutagenesis (Agilent Technologies). Plasmids were transfected into HEK-293T cells using the Lenti-X HTX packaging system (Clontech), following manufacturer's instructions. 48 hours after transfection, virus-containing culture supernatant was harvested and added to the growth medium of Tet-On 3G NIH/3T3 cells (Clontech) + 8 μg/ml polybrene (EMD Millipore). Multiple clones were isolated by direct trypsinization of single colonies, and all showed similar behavior in the centriole overduplication assay (see below).

For generation of cell lines co-expressing centrin-GFP and H2B-RFP, a human centrin-GFP construct was purchased from Origene. This plasmid and lentivirus packaging vectors (pCAG-HIVgp and pCMV-VSV-G-RSV-Rev from Hiroyuki Miyoshi, RIKEN BioResource

Center) were co-transfected into HEK-293T cells using Fugene HD (Promega). Virus was harvested as described above and added to the growth media of cells + 5-10μg/ml polybrene. A pBABE-Puro vector encoding human histone H2B C-terminally fused to mRFP1.3 was obtained from the laboratory of Don Cleveland. This plasmid and pBSK-VSV-G were co-transfected into the packaging cell line GP2-293 (Clontech) using Fugene HD. Virus was harvested as described above and added to the growth media of unsorted centrin-GFP-expressing cells + 5-10μg/ml polybrene. Populations of each cell line expressing both transgenes at moderate levels were selected by FACS.

For generation of HeLa and NIH/3T3 lines co-expressing GFP-PCNA and H2B-RFP, cells were transduced with an H2B-RFP retrovirus as described above. An MGC collection human PCNA cDNA was engineered as an N-terminal eGFP fusion and cloned into pBABE-Hygro. Retroviral production and transduction was performed as described for H2B-RFP above. Populations of each cell line expressing both transgenes at moderate levels were selected by FACS.

For generation of RPE1 cells with a Plk4(G95L) knock-in, we targeted the intronic region between exons 4 and 5 of the Plk4 locus with a gRNA sequence (GGAAGCTGAGTGTTAAGTTC) cloned into pX458 (a gift from Feng Zhang; Addgene plasmid #48138; *44*). A repair template was cloned to introduce the G95L point mutation, as well as a neomycin resistance cassette within the intronic region (see **Fig. S11**). RPE1 cells were transfected with the Cas9/gRNA plasmid, then transduced with adeno-associated virus coding for the repair template using previously described methods (*45*). Cells were selected in 96-well plates for 2 weeks using 0.5 mg/ml Geneticin (Life Technologies). Positive clones homozygous for the G95L knock-in were identified by PCR and sequencing of genomic DNA.

For generation of RPE1 cells expressing a constitutive LATS1/LATS2 microRNA, the pLenti-EmGFP-LATS1/2KD plasmid was used (a gift from Yutaka Hata; Addgene plasmid #52085; *46*). Lentiviral generation and transduction were performed as described above. Transduced cells were selected by FACS based on GFP fluorescence.

For generation of RPE1 cells expressing a constitutive p53 shRNA, lentivirus coding for either Glu4 control or p53 shRNA were gifts from Quan Zhu and Inder Verma. Lentiviral transduction were performed as described above. Transduced cells were used directly in experiments as the transduction efficiency was >95% for both control and p53 shRNA lentiviruses.

Centriole depletion assay for compound screening

1,500 NIH/3T3 cells or 3,500 HCT116 cells were seeded into 96-well SCREENSTAR microplates (Greiner) and treated with inhibitors in dose response, added from DMSO stocks. After 3 days, cells were fixed directly in the wells with 100% methanol (-20°C, 10 minutes). The fixed cells were washed with PBS and stained with primary antibodies against γ-tubulin and, for a subset of compounds, Cep192. Cells were then stained with Alexa-488 donkey anti-mouse and Alexa-647 goat anti-rabbit secondary antibodies. Cells were imaged using either a Model 500 LumaScope (Etaluma) or an EVOS FL (Advanced Microscopy Group/Life Technologies), and centriole depletion was determined by scoring the percentage of cells without visible γ-tubulin/Cep192 foci.

Quantification of centrosome numbers from fixed samples

Cells were seeded onto poly-D-lysine-coated coverslips (Neuvitro) in 12-well plates at least 8 hours before fixation. At the required timepoints for each experiment, cells were washed once with PBS and fixed in 100% methanol (-20°C, 5 minutes). Fixed cells were washed with PBS, blocked with PBS + 4% BSA + 0.1% Triton X-100, and stained with primary antibodies against γ-tubulin and Cep192, which localize to the pericentriolar material and proximal to the outer centriole wall, respectively (*47,48*). Alexa488-labeled anti-mouse secondary antibody (against anti-γ-tubulin) and Alexa647-labeled anti-rabbit secondary antibody (against anti-Cep192) were both used at 1.5 μg/mL. Samples were mounted onto slides with Prolong Gold antifade reagent (Life Technologies). Images of fixed interphase cells were acquired on a Nikon Eclipse E800 with a 60X 1.4 NA PlanApo objective and ORCA-ER camera (Hamamatsu) using Metamorph software (Molecular Devices). Quantification of foci was performed manually. A focus was defined as a bona-fide centrosome if it was positive for both γ-tubulin and Cep192 (true for >95% of foci).

Microtubule regrowth assay

NIH/3T3 cells were treated with DMSO or 300 nM centrinone for >2 weeks prior to the start of the experiment. Cells were seeded onto coverslips in 12-well plates and treated with 16 μM nocodazole for 4 hours to depolymerize microtubules. Wells were washed 6 times with PBS to remove the nocodazole, and fresh, pre-warmed medium was added to each well. After 5 minutes of recovery, cells were fixed with 100% methanol (-20°C, 5 minutes) and stained with antibodies against γ-tubulin and α-tubulin. Coverslips were mounted onto slides and imaged on a DeltaVision microscope (Applied Precision) with a 60X 1.42 NA PlanApo objective and CoolSnap camera (Photometrics). Image deconvolution was performed in softWoRx (Applied Precision) and subsequent processing was performed in ImageJ (NIH).

Cilia formation assay in NIH/3T3 cells

NIH/3T3 cells were treated with DMSO or 300 nM centrinone for >2 weeks prior to the start of the experiment. Cells were seeded onto coverslips and starved for 40 hours by replacing their media with DMEM + 0.5% defined bovine serum. Cells were then washed with PBS, fixed with 100% methanol (-20°C, 5 minutes), stained with antibodies against γ-tubulin and IFT-88, and mounted onto slides. Image acquisition and deconvolution were performed on the DeltaVision system, as above. Subsequent image processing was performed in ImageJ.

Multiciliation assay in *Xenopus* embryos

Xenopus embryos were obtained by in vitro fertilization using standard protocols (*49*) approved by the Northwestern University Institutional Animal Care and Use Committee. Fertilized *Xenopus* embryos were injected with mRNA encoding the centriole marker Centrin4-GFP (333 pg/embryo) and a Dexamethasone-inducible Multicilin (hGR 3'MCI; 160 pg/embryo) (*50, 51*). Embryos were allowed to develop to stage 10.5-11 and were then treated with a combination of Dexamethosone (20 □M) and either DMSO, centrinone or centrinone-B. Drug treatments were performed in 0.5X Marc's Modified Ringers (2.5 mM HEPES, 55 mM NaCl, 1 mM KCl, 0.5 mM $MgCl_2$, 1 mM $CaCl_2$, 1 mM $NaHCO_3$, pH 7.8) with 4% Ficoll to facilitate solubility. Embryos were treated for 13 hours at room temperature, fixed in 4% paraformaldehyde and treated with the actin stain phalloidin. Confocal image stacks were collected using a Nikon A1R microscope and centriole numbers were manually quantified in Nikon Elements software. For

each condition, centriole numbers were quantified from approximately 100 cells from at least 3 embryos.

Centriole overduplication assay

Tet-On 3G NIH/3T3 cells (Clontech) stably transduced with GFP, Plk4-GFP or Plk4(G95L)-GFP were seeded onto coverslips in a 12-well plate at 30,000 cells/well. Transgene expression was induced with 1 μg/ml doxycycline. At the same time, cells were treated with DMSO or 300 nM centrinone. Treated cells were incubated for 40 hours, and then washed with PBS and fixed in 100% methanol (-20°C, 5 minutes). Fixed samples were stained for γ-tubulin and Cep192, and mounted onto slides. Image acquisition and deconvolution were performed on the DeltaVision system equipped with a 100X 1.3 NA U-PlanApo objective. Subsequent image processing was performed in ImageJ.

Quantification of Aurora A and Aurora B activity

HeLa cells were seeded onto coverslips, and allowed to settle for 16 hours. Cells were then treated with DMSO, 125 nM centrinone or 1 μM VX-680 for 7 hours. For quantification of Aurora A activity, treated cells were fixed in 100% methanol (-20°C, 5 minutes) and stained with anti-p-LATS2(Ser83) and Hoechst 33342. 5 x 1 μm z-sections of metaphase cells (or in the case of VX-680-treatment, cells with condensed DNA) were acquired on the DeltaVision system with the 60X 1.42 NA PlanApo objective. Stacks were projected and transferred to ImageJ for analysis. The integrated signal from a 1 x 1 μm box centered on each centrosome was measured. For background subtraction, a 1 x 1 μm box in the cytoplasm was used. Mean values of measurements were normalized to the DMSO-treated condition. For quantification of Aurora B activity, treated cells were fixed in 4% paraformaldehyde for 15 minutes at room temperature, then permeabilized with PBS + 0.25% Triton X-100 for 5 minutes. Fixed cells were stained with anti-p-H3(Ser10), anti-α-tubulin, and Hoechst 33342. 5 x 1 μm z-sections were acquired as above and projected. The DNA signal was used to threshold and define a binary mask, which was then transferred to the p-H3 channel. The mean intensity of this region was measured in the p-H3 channel. For background subtraction, the masked region was expanded by 20 pixels, and the mean intensity of the peripheral region was used. Mean values of measurements were normalized to the DMSO-treated condition.

Proliferation assays

For each condition, cells were seeded in triplicate into 6-well plates at 50,000 cells/well. Compounds were added at the indicated concentrations. At 24-hour intervals, 3 wells were harvested per condition. Cell counting was performed using a TC10 automated cell counter (Bio-Rad). Results are from 3 independent experiments.

Passaging assays

Cells were seeded into 10 cm tissue culture plates at 150,000 (HeLa, NIH/3T3 and RPE1) or 200,000 cells/plate (primary fibroblasts). Compounds were added at the indicated concentrations. At 4-day intervals, cells were harvested, counted using a TC10 cell counter, and re-seeded into new plates at the densities above. Results are from 2 independent experiments.

Analysis of cell cycle progression

HeLa and NIH/3T3 cells co-expressing GFP-PCNA and H2B-RFP were treated with DMSO or centrinone (125 nM for HeLa, 300 nM for NIH/3T3) for >2 weeks prior to the start of the experiment. Cells were seeded into 96-well cycloolefin plates (Greiner Bio-One) at 4000 cells/well, 8-10 hours before imaging. Movies were acquired on a CV1000 spinning disk confocal system (Yokogawa Electric Corporation) with a 20X 0.75 NA U-PlanApo objective and 512x512 EM-CCD camera (Hamamatsu). The imaging chamber was maintained at 37°C and 5% CO_2. Image acquisition and data analysis were performed using CellVoyager software. 12-24 fields/well were imaged, with duplicate wells for each condition. 3 x 4 μm z-sections in the GFP (20% power, 100 ms, 25% gain) and RFP (25% power, 100 ms, 25% gain) channels were captured in each field, at 10-minute intervals for 48 hours. Cells were manually tracked from the beginning of G1 (chromosome decondensation) to the beginning of the next mitosis (nuclear envelope breakdown). GFP-PCNA foci appear in the nucleus during mid- to late-S-phase, and the first frame in which these foci are no longer visible was defined as the beginning of G2 phase. Results represent combined measurements of 200 cells per condition from 2 independent experiments.

Analysis of mitosis and daughter cell fate

HeLa, NIH/3T3 and RPE1 cells co-expressing centrin-GFP and H2B-RFP were treated with DMSO or centrinone (125 nM for HeLa and RPE1, 300 nM for NIH/3T3) beginning 2 days, 1 day or immediately prior to imaging to capture 0-, 1-, and 2-centrosome mitoses, respectively. Cells were seeded into 96-well cycloolefin plates at 5000 cells/well, 8-10 hours before imaging. Movies were acquired on the CV1000 with a 40X 0.95 NA U-PlanApo objective. The imaging chamber was maintained at 37°C and 5% CO_2. Image acquisition and data analysis were performed using CellVoyager software. 20 fields/well were imaged. For HeLa and NIH/3T3 cells, 5 x 2 μm z-sections in the GFP (25% power, 125 ms, 30% gain) and RFP (25% power, 100 ms, 30% gain) channels were captured in each field, at 5-minute intervals for 24 hours. For RPE1 cells, 5 x 2 μm z-sections in the GFP (20% power, 100 ms, 30% gain) and RFP (25% power, 100 ms, 30% gain) channels were captured in each field, at 5-minute intervals for 8 hours. To track RPE1 daughter cell fate, imaging was then switched to 3 x 4 μm z-sections in the RFP channel only, at 10-minute intervals for 48 hours. Mitosis was measured from nuclear envelope breakdown to anaphase onset (or arrest). Results represent combined measurements of 100 mother cells per condition from 2-4 independent experiments.

To study the correlation between mother cell prometaphase duration and daughter cell fate, RPE1 cells co-expressing centrin-GFP and H2B-RFP were seeded into 96-well cycloolefin plates at 5000 cells/well, 8-10 hours before imaging. Cells were treated with 80 nM nocodazole and immediately imaged on the CV1000 system with a 40X 0.95 NA U-PlanApo objective. The imaging chamber was maintained at 37°C and 5% CO_2. 20 fields/well were imaged. 5 x 2 μm z-sections in the GFP (20% power, 100 ms, 30% gain) and RFP (25% power, 100 ms, 30% gain) channels were captured in each field, at 5-minute intervals for 6 hours. The plate was then removed from the microscope, and wells were washed 6 times with warm medium. The plate was returned to the microscope, and imaging was resumed, capturing 3 x 4 μm z-sections in the RFP channel only, at 10-minute intervals for 50 hours. To study the effect of chromosome missegregation on daughter cell fate, cells were treated with 1 μM NMS-P715 to inhibit the spindle assembly checkpoint kinase Mps1, then imaged as described above. Only mitotic events with clear missegregation (lagging chromosomes and subsequent formation of daughter cells

with micronuclei) were analyzed. For both experiments, results represent combined measurements of 100 mother cells from 2 independent experiments.

Live imaging of centriole recovery

HeLa cells co-expressing centrin-GFP and H2B-RFP were treated with 125 nM centrinone for >2 weeks prior to the start of the experiment. Centrinone was washed out 39 hours, 15 hours, or immediately prior to imaging to obtain data within a large time window of centriole recovery. Cells were seeded into 96-well cycloolefin plates at 5000 cells/well, 8-10 hours before imaging. Movies were acquired on the CV1000 with a 40X 0.95 NA U-PlanApo objective. The imaging chamber was maintained at 37°C and 5% CO_2. Image acquisition and data analysis were performed using CellVoyager software. 20 fields/well were imaged. 5 x 2 μm z-sections in the GFP (25% power, 125 ms, 30% gain) and RFP (25% power, 100 ms, 30% gain) channels were captured in each field, at 10-minute intervals for 72 hours. For each cell, centrin foci were counted at nuclear envelope breakdown, when the centrosomes maximally separate from each other. Results represent combined measurements of 300 mother cells from 3 independent experiments.

Apoptosis assay

HeLa and NIH/3T3 cells were treated with DMSO or centrinone (125 nM for HeLa, 300 nM for NIH/3T3) for 8 days prior to the start of the experiment. Cells were seeded into 96-well cycloolefin plates (Greiner Bio-One) 20 hours before imaging. 30 minutes before imaging, cells were stained with NucRed Live 647 (Life Technologies) and CellEvent Caspase-3/7 Green Reagent (Life Technologies) to mark DNA and apoptotic cells, respectively. Images were acquired on a CV7000 spinning disk confocal system (Yokogawa Electric Corporation) with a 20X 0.75 NA U-PlanApo objective and 2560x2160 sCMOS camera (Andor) at 2x2 binning. The imaging chamber was maintained at 37°C and 5% CO_2. Image acquisition and data analysis were performed using CV7000 software. 9 fields/well were imaged, with triplicate wells for each condition. 10 x 2 μm z-sections in the green (25% power, 100 ms, 2.2X gain) and far-red (30% power, 200 ms, 2.2X gain) channels were captured in each field. The percentage of apoptotic cells was calculated by manual counting of cells positively or negatively staining with the fluorescent caspase reporter. Results represent combined measurements from 2 independent experiments.

Flow cytometry

Cells were seeded into 15 cm tissue culture plates such that each plate was 50-80% confluent at the time of harvesting. Cells were de-adhered by trypsinization and pelleted in 15 ml tubes by centrifugation. Each pellet was resuspended in 0.3 mL PBS, and 0.7 mL ice-cold 100% ethanol was added to the tube while gently vortexing. Fixed cells were stored at 4°C for up to 2 weeks. For DNA content analysis, fixed cells were pelleted, washed twice with PBS, and resuspended in 0.5 mL PBS + 2% BSA and Alexa488-conjugated anti-p-H3(Ser10) antibody. Samples were incubated for 1 hour at 4°C, then washed twice with PBS + 2% BSA. Pellets were resuspended in 1 mL PBS + 2% BSA, 10 μg/ml propidium iodide (Sigma-Aldrich), 50μg/ml RNAse A (Thermo Scientific). Samples were incubated at 37°C for 30 minutes, then transferred to 12x75 mm tubes for analysis. Data were acquired using FACSDiva software on a LSR II flow cytometer (BD Biosciences). 50,000 cells were analyzed per condition. Cell cycle fitting was performed using ModFit LT (Verity Software House).

DNA Damage Checkpoint Assay

HeLa and NIH/3T3 cells were treated with DMSO or centrinone (125 nM for Hela, 300 nM for NIH/3T3) for >2 weeks prior to the start of the experiment. Cells were seeded into 10 cm tissue culture plates at 30-40% confluence 24 hours before the experiment. For the positive control, cells were pre-treated with 5 mM caffeine (Sigma-Aldrich) for 1 hour before beginning the experiment. Cells were treated with 2 μM doxorubicin for 90 minutes, then washed twice with PBS and allowed to recover in fresh medium for 3 hours (with 5 mM caffeine, where indicated). Cells were then harvested and processed for flow cytometry as described above.

γ-H2A.X staining

RPE1 cells were treated with DMSO or 125 nM centrinone for 4 days. Cells were either seeded onto coverslips for staining, or harvested for cell extracts (see below). Cells treated for 16 hours with 0.5 μM doxorubicin were used as a positive control for DNA damage induction. Coverslips with cells were fixed in 100% methanol (-20°C, 5 minutes) and stained with antibodies against γ-H2A.X, γ-tubulin, and Hoechst 33342. Coverslips were mounted onto slides and imaged on the DeltaVision system at 100X magnification. Cells with γ-H2A.X foci in the nucleus were manually counted for each condition.

MAPKAPK-2 activation assay

RPE1 cells on 10 cm plates were treated with DMSO or 10 μM SB203580 for 2 hours prior to induction of stress. To induce osmotic stress, the growth medium was replaced with 0.5 M sorbitol (with DMSO or 10 μM SB203580) for 45 minutes before harvesting for Western blotting (see below).

Plk4 stabilization assay

Expression was induced in Plk4-YFP DLD-1 cells using 1 μg/ml doxycycline. At the same time, cells were treated with the indicated concentrations of compounds. Cells were incubated for 24 hours before harvesting for Western blotting (see below).

Western blotting

Asynchronously growing cells from 10 cm plates were harvested at 50-80% confluence and lysed by sonication in RIPA buffer + protease and phosphatase inhibitor cocktail (Thermo Scientific). Cell extracts were stored at -80°C until use. Before use, concentrations of extracts were normalized using a Bio-Rad Protein Assay (Bio-Rad). For every sample, 25-50 μg protein/lane was run on Mini-PROTEAN gels (Bio-Rad), and transferred to PVDF membranes using a TransBlot Turbo system (Bio-Rad).

For p53, p-p53(S33), p-p53(S392), p-p38(T180/Y182), acetyl-p53(K382), LATS2, YAP, MDM2, MAPKAPK-2 and GFP, blocking and antibody incubations were performed in TBS-T + 5% non-fat dry milk. For p-YAP(S127), p-p53(S9), p-p53(S15), p-p53(S20), p-p53(S37), p-p53(S315), p21 and p-MAPKAPK-2(T334), blocking and antibody incubations were performed in TBS-T + 5% BSA. Detection was performed using HRP-conjugated secondary antibodies (GE Healthcare) with WesternBright Sirius (Advansta) or SuperSignal West Femto (Thermo Scientific) substrates. Membranes were imaged on a ChemiDoc MP system (Bio-Rad). Membranes were stripped and reprobed with antibodies against α-tubulin or GAPDH as loading controls.

Tetraploid cell arrest assay

RPE1 Fucci cells expressing wild-type or constitutively-active (S5A) YAP were seeded into a 96-well cycloolefin plate at 3000 cells/well, 16 hours before treatment. Cells were treated with DMSO or 4 μM cytochalasin D (Sigma-Aldrich) for 24 hours, then washed 5 times with warm medium. 12 hours after drug washout, the plate was imaged on the CV1000 system with a 10X 0.4 NA U-PlanApo objective. Image acquisition and data analysis were performed using CellVoyager software. 4 fields/well were imaged, with 12 wells for each condition. 4 x 4 μm z-sections in the GFP (25% power, 100 ms, 30% gain) and RFP (30% power, 150 ms, 60% gain) channels were captured in each field. Tetraploid cells were identified as cells with two nuclei. The number of cells in G1 (*red nuclei*, expressing hCdt-1-mCherry) and S/G2 (*green nuclei*, expressing hGem-Azami-Green) was quantified, and the percentage of cells in G1 calculated.

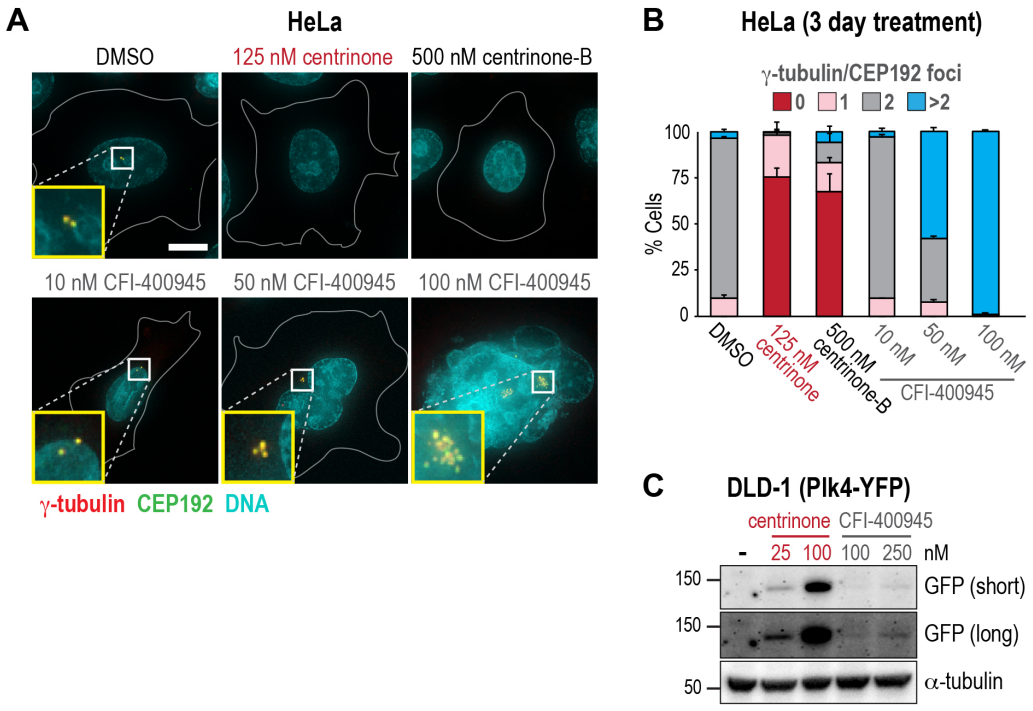

Figure S1. CFI-400945 is a non-selective Plk4 inhibitor that does not deplete centrioles from cells

Treatment of HeLa cells with 50 or 100 nM CFI-400945 causes centrosome amplification, likely due to partial blockade of Plk4 autophosphorylation-mediated degradation (*52*). At these concentrations, CFI-400945-treated cells also become grossly multinuclear (see examples in *A*) and stop dividing, presumably due to Aurora B inhibition (*18,19*). (**A**) Deconvolved wide-field images of HeLa cells treated for 3 days with DMSO, centrinone, centrinone-B, or CFI-400945. Cells were fixed and stained for γ-tubulin and Cep192. Images are maximum intensity projections. Cell boundaries are outlined in gray. Insets are 3.4X magnified. Scale bar, 10 μm. (**B**) Quantification of γ-tubulin/Cep192 foci from cells in *A*. Data are mean +/- SD (*N*=3). Results similar to those described in *A* and *B* for HeLa cells were also observed in mouse NIH/3T3 fibroblasts as well as human breast (MDA-MB-231 and MDA-MB-468) and colon (HCT-116) carcinoma cells. (**C**) Western Blot of DLD-1 cells induced to overexpress full-length mouse Plk4-YFP (*53*), treated with the indicated centrinone or CFI-400945 concentrations for 24 hours. In untreated cells, levels of overexpressed Plk4-YFP are limited by autophophorylation-induced degradation. Inhibition of Plk4 kinase activity leads to Plk4-YFP stabilization. At 250 nM CFI-400945, only slight Plk4-YFP stabilization is observed compared to the more substantial stabilization seen in the presence of 25 nM or 100 nM centrinone.

Wong et al. Figure S2

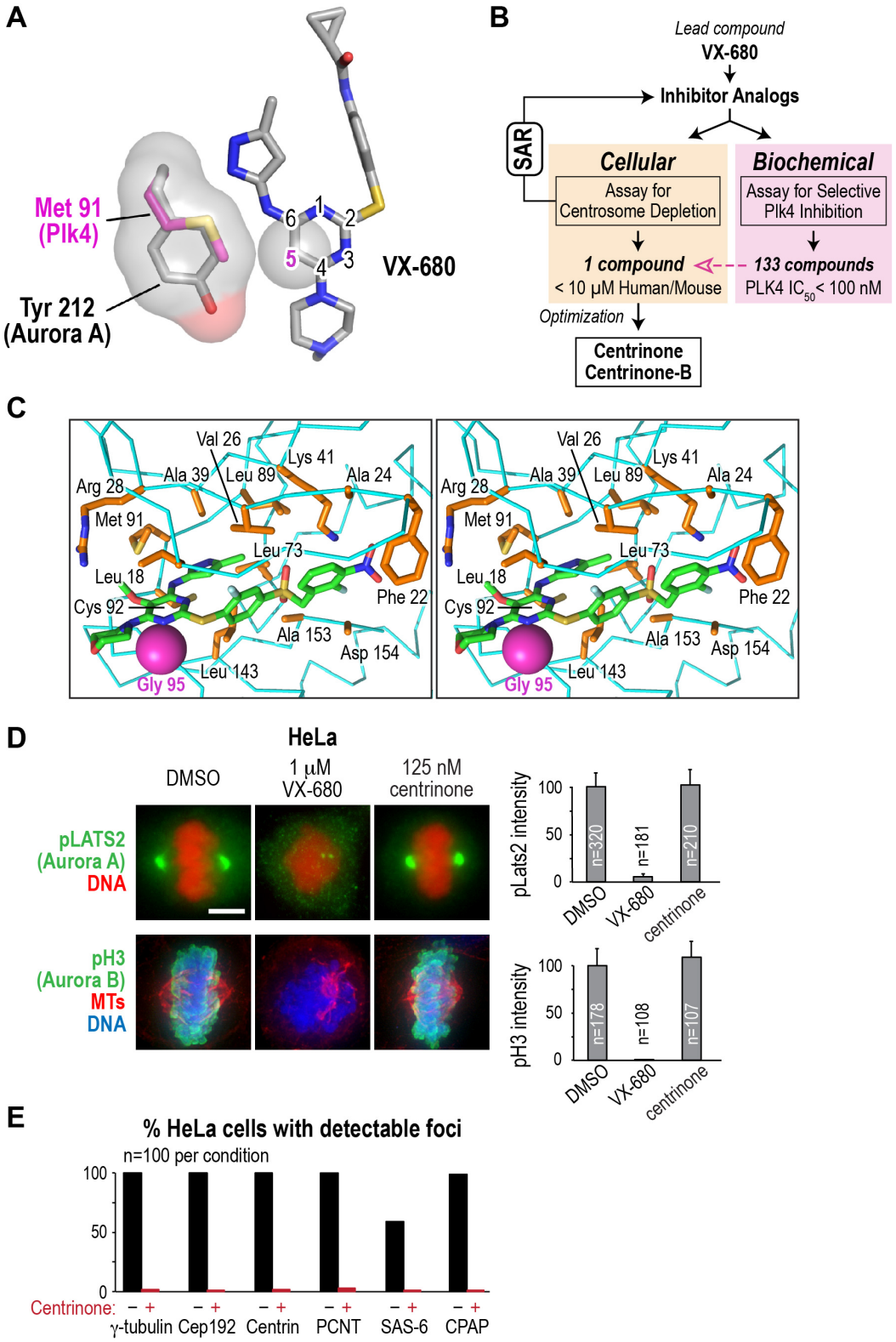

Figure S2. Centrinone is a selective Plk4 inhibitor that depletes centrioles from cells
(**A**) Selection of VX-680 as the lead compound and selectivity design strategy. Inspection of a previously deposited structure of the Plk4 kinase domain bound to AMP-PNP (PDB:3COK) revealed an uncommon residue (Met 91) in the hinge region connecting the two kinase domain lobes. Hinge interactions can account for 40-60% of the binding energy of certain classes of ATP-competitive kinase inhibitors (*54*), and this region has previously been successfully targeted to generate selective inhibitors (e.g. the Plk1 inhibitor BI2356; *55*). Modeling of reported biochemical Plk4 inhibitors predicted that the Aurora kinase inhibitor VX-680 would bind with its pyrimidine ring adjacent to Met 91. We hypothesized that selectivity for Plk4 could be introduced into this scaffold by adding substituents to the C5 ring position that would be accommodated by the flexible Met 91 of Plk4, but not by the bulkier tyrosine residues at the equivalent positions in human Aurora A/B/C. The image shown here was generated by superimposing the structure of human Aurora A bound to VX-680 (PDB:3E5A) over that of Plk4 bound to AMPPNP (PDB:3COK). The C5 position of VX-680 (***gray sphere***), Tyr 212 of Aurora A (***gray sticks and surface***), and Met 91 of Plk4 (***magenta sticks***) are highlighted. (**B**) Flowchart illustrating the centrinone development process. Using VX-680 as a starting point, inhibitor analogs were iteratively synthesized based on the structure-activity relationship (SAR) results from cellular centrosome depletion and biochemical Plk4 and Aurora A/B kinase inhibition assays. Only one of the 133 compounds that robustly inhibited Plk4 *in vitro* (LCR-015) depleted centrosomes from both human and mouse cells at <10 μM. This result validated our approach of monitoring cellular activity in parallel with biochemical potency. LCR-015 was further optimized for potency and selectivity, resulting in centrinone and centrinone-B. (**C**) Stereo diagram of centrinone in the Plk4 active site showing a Cα trace of the Plk4 main chain ***(cyan)***, and residues whose side chains form nonpolar contacts ***(orange)*** with centrinone ***(green)***. The Cα of Gly 95 ***(magenta sphere)*** is packed against centrinone. Mutation of this residue to a bulky leucine preserves in vitro catalytic activity but severely compromises centrinone binding. The benzylsulfone moiety inserts itself between the side chain of the catalytic lysine (Lys 41) and the aspartic acid (Asp 154) of the DFG motif. The side chain of Asp 154 is not visible in the electron density so it has been modeled as an alanine. (**D**) HeLa cells treated with DMSO, VX-680, or centrinone for 7 hours. Cells were fixed and stained for p-LATS2(S83) and p-H3(S10), which are reporters of Aurora A and Aurora B activity, respectively. Scale bar, 5 μm. The mean intensities of p-LATS2 and p-H3 staining were quantified for the three conditions. Values are normalized to DMSO. Data are mean +/- SD (*N*=3). (**E**) Quantification of the number of cells with detectable foci in HeLa cells stained for centriolar (centrin, SAS-6, CPAP) and pericentriolar material (γ-tubulin, Cep192, PCNT) proteins. Centrinone treatment resulted in loss of all markers from cells.

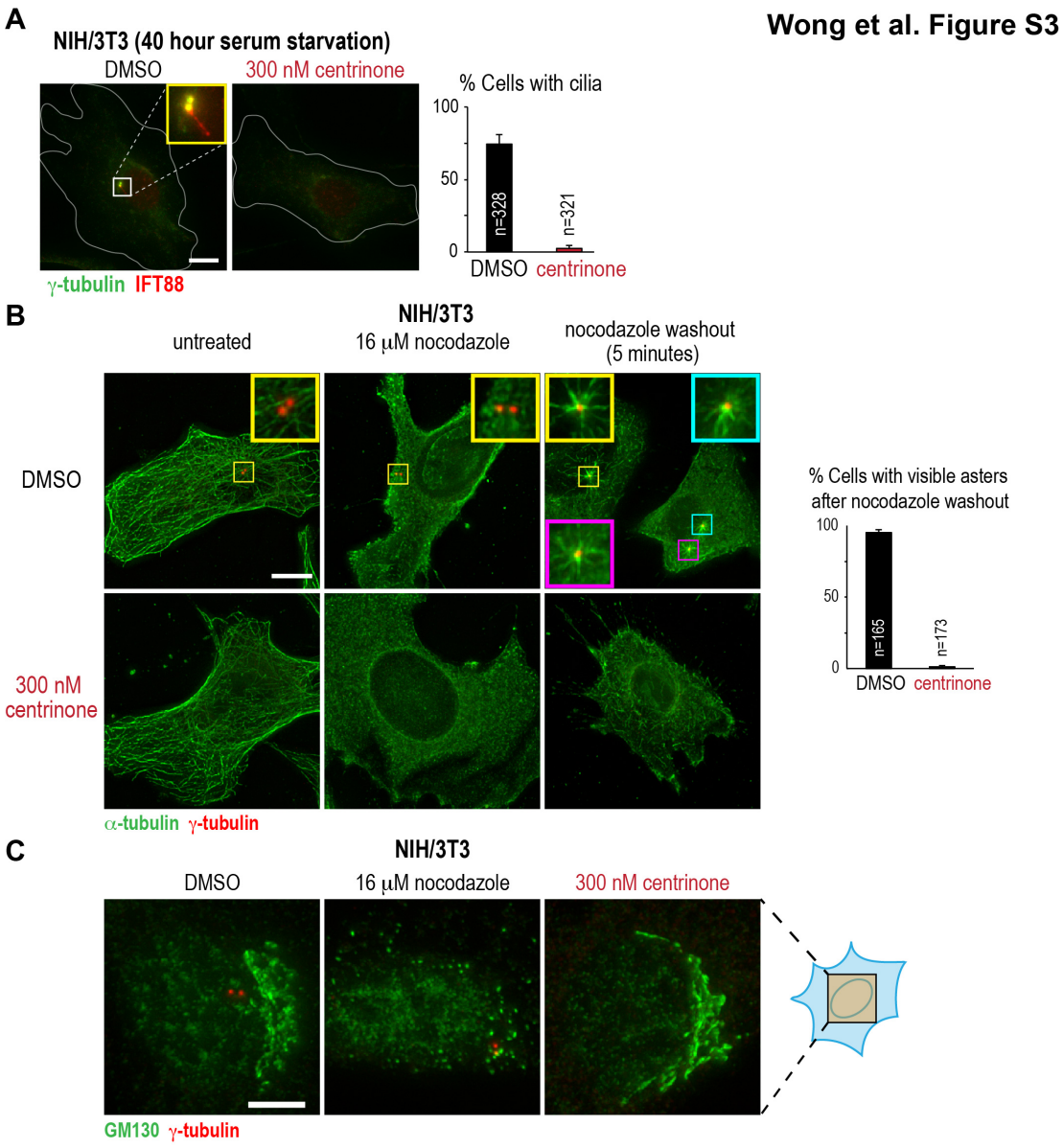

Figure S3. Centrinone prevents assembly of primary cilia and centrosomal microtubule-organizing centers but Golgi organization is largely normal

(**A**) Serum-starved DMSO- and centrinone-treated NIH/3T3 cells stained for γ-tubulin and the ciliary marker IFT88. Inset is 3.4X magnified. Scale bar, 10 μm. The mean percentage of cells with cilia was quantified. Data are mean +/- SD (*N*=3). (**B**) Deconvolved wide-field images of DMSO- and centrinone-treated NIH/3T3 cells either untreated, in the presence of 16 μM nocodazole or 5 minutes after nocodazole washout. Maximum intensity projections are shown. In the absence of centrosomes, short microtubules form throughout the cytoplasm after nocodazole washout, instead of focused asters. Insets are 3.3X magnified. Scale bar, 10 μm. The mean percentage of cells with visible asters 5 minutes after nocodazole washout was quantified. Data are mean +/- SD (*N*=3). (**C**) Golgi staining in NIH/3T3 cells treated with DMSO or centrinone for 10 days. Nocodazole treatment was used as a positive control for Golgi dispersal. Scale bar, 5 μm. Similar results were obtained in HeLa cells.

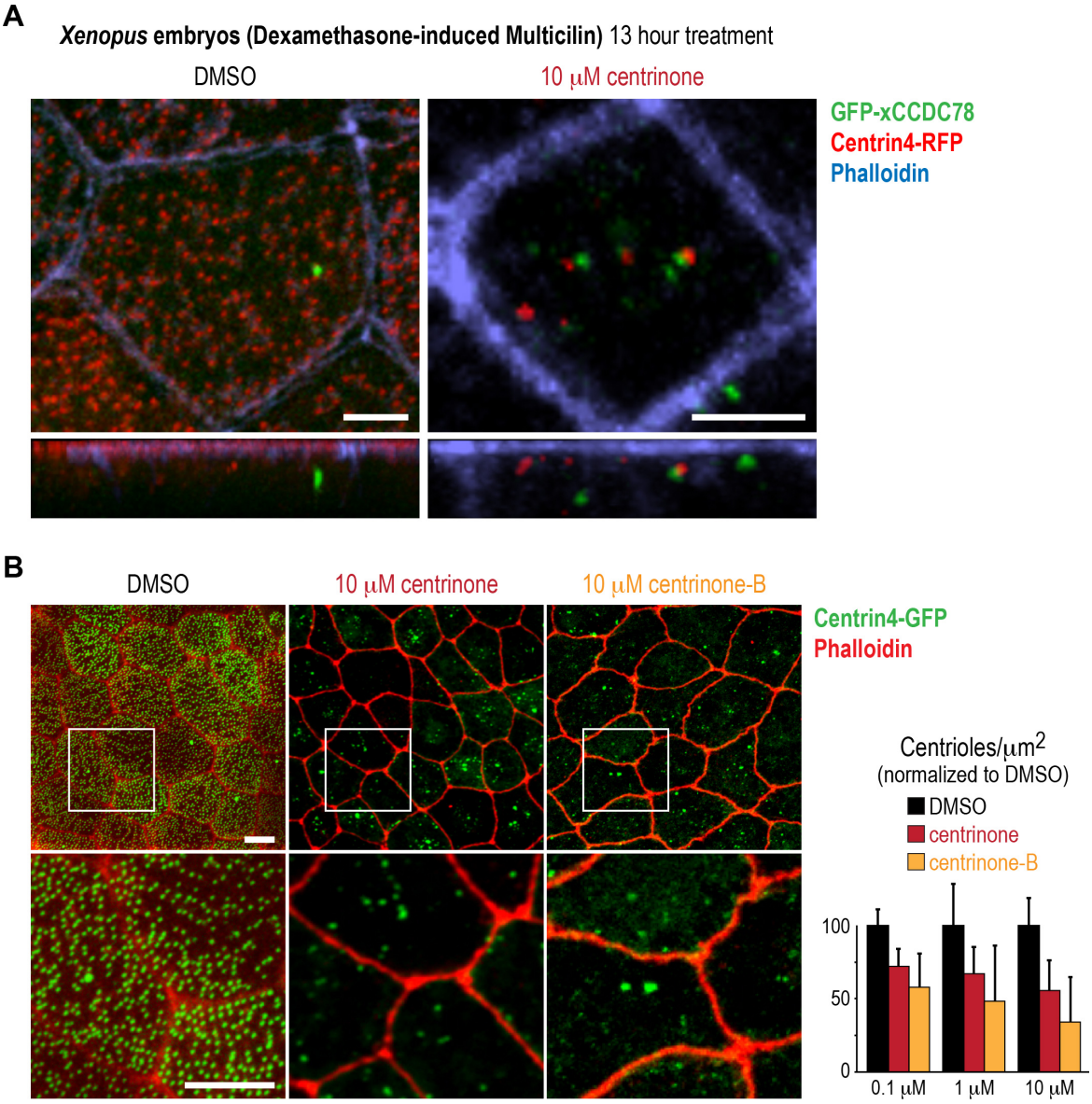

Figure S4. Centrinone inhibits centriole assembly in *Xenopus* multiciliated cells

Dexamethasone-induced Multicilin expression leads to the formation of ectopic multiciliated cells that cover the entire ectoderm in *Xenopus* embryos (*50*). These cells contain numerous centrioles that are primarily generated from structures called deuterosomes that are marked by xCCDC78 and also recruit Plk4 (*51*). (**A**) Fluorescence confocal images of multiciliated cells treated with DMSO (control) or 10 μM centrinone expressing GFP-xCCDC78 and Centrin4-RFP and stained with Phalloidin to mark cell boundaries indicate that deuterosomes are present in centrinone-treated cells. Scale bar, 5 μm. (**B**) Fluorescence confocal images of DMSO, centrinone, and centrinone-B-treated multiciliated cells expressing Centrin4-GFP and stained with Phalloidin. Boxed regions are 3X magnified. Scale bars, 10 μm. Graph quantifying centriole density after treatment with DMSO or the indicated concentations of centrinone or centrionone-B. Centrinone-treated cells exhibit dramatically reduced centriole numbers, suggesting that centriole assembly in multiciliated cells is Plk4-dependent. Data are mean +/- SD (*N*=3).

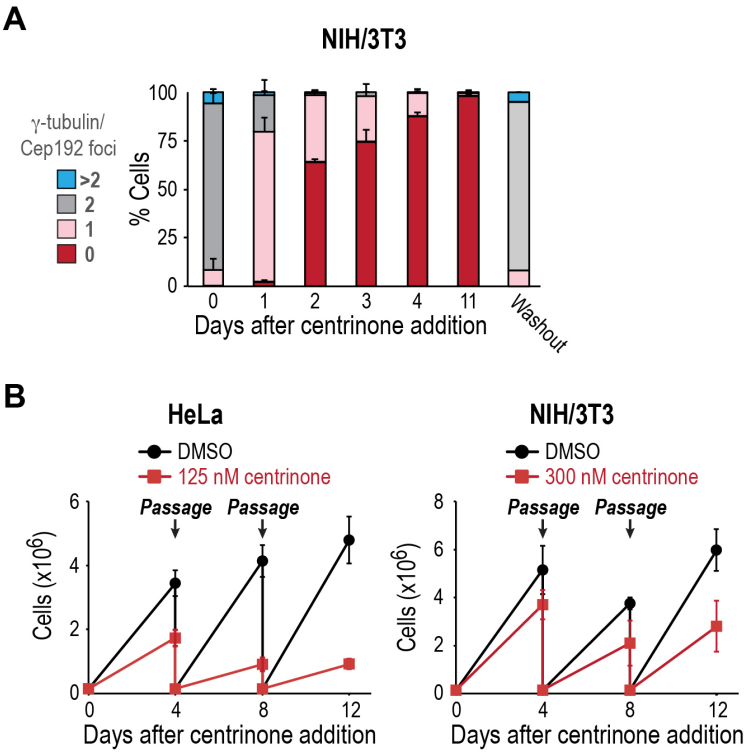

Figure S5. HeLa and NIH/3T3 cells proliferate indefinitely without centrosomes
(**A**) Centrosome depletion kinetics immediately following centrinone addition to NIH/3T3 cells. Data are mean +/- SD (*N*=3). (**B**) Passaging assay of HeLa and NIH/3T3 cells beginning immediately after centrinone addition. Cells were passaged at the indicated intervals. Centrinone-treated cells continue proliferating indefinitely, albeit at a slower rate than control cells. Data are mean +/- SD (*N*=2).

Wong et al. Figure S6

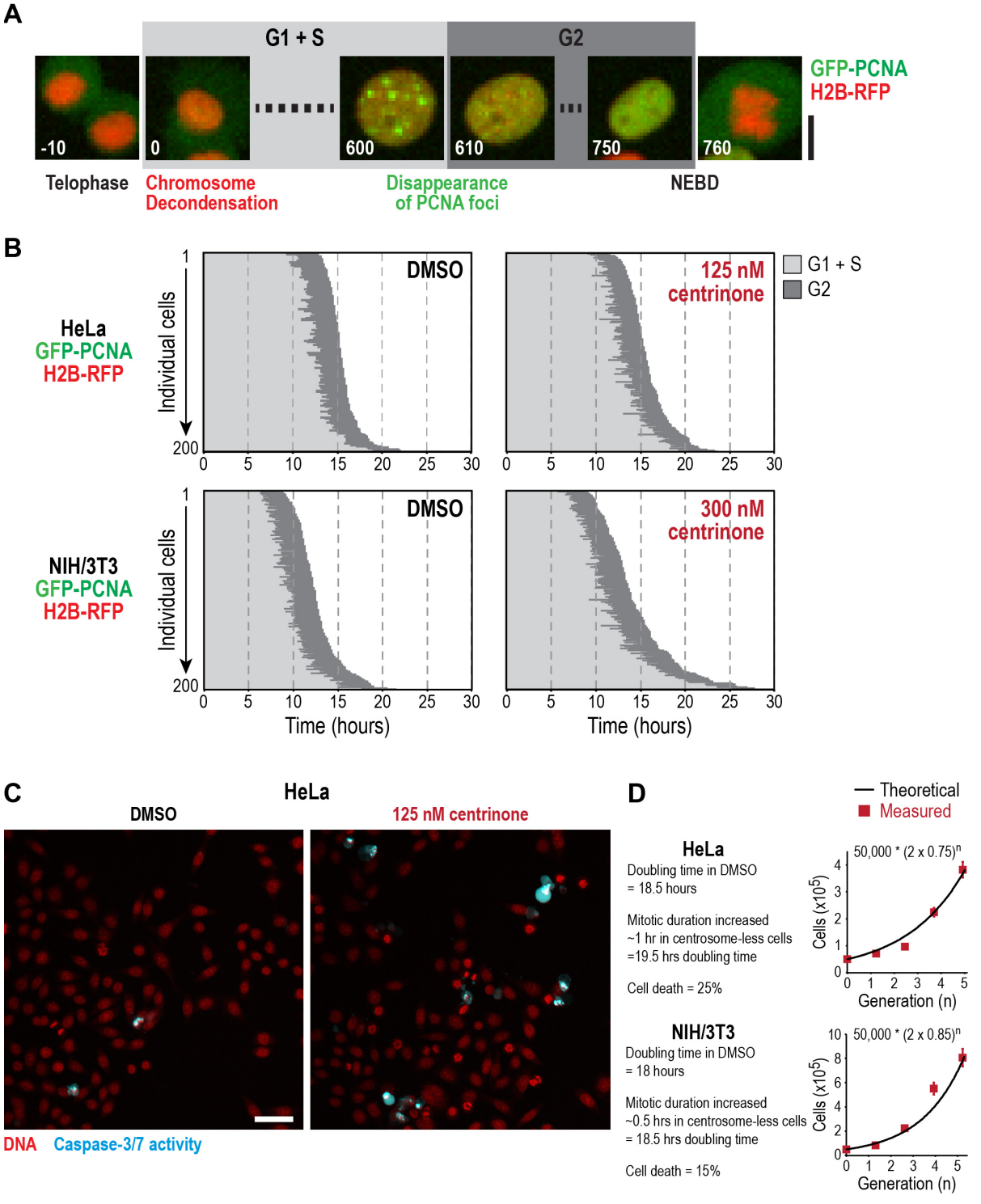

Figure S6. Centrosome loss does not affect interphase duration but leads to an increase in apoptotic cell death

To determine how centrosome removal led to a reduction in population growth, we first analyzed whether centrosome-less cells exhibit altered progression through interphase. We measured the duration of G1+S and G2 in control and centrosome-less HeLa and NIH/3T3 cells engineered to co-express GFP-PCNA and H2B-RFP. The H2B-RFP enables monitoring chromosome decondensation and nuclear envelope breakdown (NEBD), which mark the M/G1 and G2/M transitions, respectively. GFP-PCNA localizes to nuclear foci representing sites of active DNA replication that form during S-phase and persist until the S/G2 boundary (*56*), enabling assessment of the end of S phase. (**A**) Confocal images (maximum intensity projections) illustrating how cell cycle intervals (G1+S and G2) were measured. Times in the bottom left of each panel are in minutes relative to the beginning of G1 (chromosome decondensation). Scale bar, 10 μm. (**B**) Plots showing G1+S and G2 durations in DMSO- and centrinone-treated HeLa and NIH/3T3 cells co-expressing GFP-PCNA and H2B-RFP. Horizontal bars represent measurements from individual cells, ordered by total interphase duration. *N*=2. (**C**) Confocal images (maximum intensity projections) of HeLa cells treated with DMSO or centrinone for 8 days, then stained for apoptotic cells using a fluorescent caspase-3/7 activity reporter substrate. Scale bar, 50 μm. The percentage of dying cells is underestimated by this assay because it does not account for the fragile cells that have detached from the surface (in particular, those that die during or shortly after mitosis while the cell is loosely adherent). (**D**) Theoretical proliferation curves (black) for HeLa and NIH/3T3 cells with the indicated percentages of cell death, compared to measurements of centrinone-treated cells (red squares; data reproduced from **Fig. 2B**). The equations used to generate the curves are shown above each plot (50,000 = starting cell number; n = generation number). The doubling times were calculated by best-fit exponential regression of proliferation data from DMSO-treated cells adjusted as shown for increased time spent in mitosis. The curves indicate that the reduced proliferation rate of centrosome-less HeLa and NIH/3T3 cells can be explained by 25% and 15% cell death per generation, respectively.

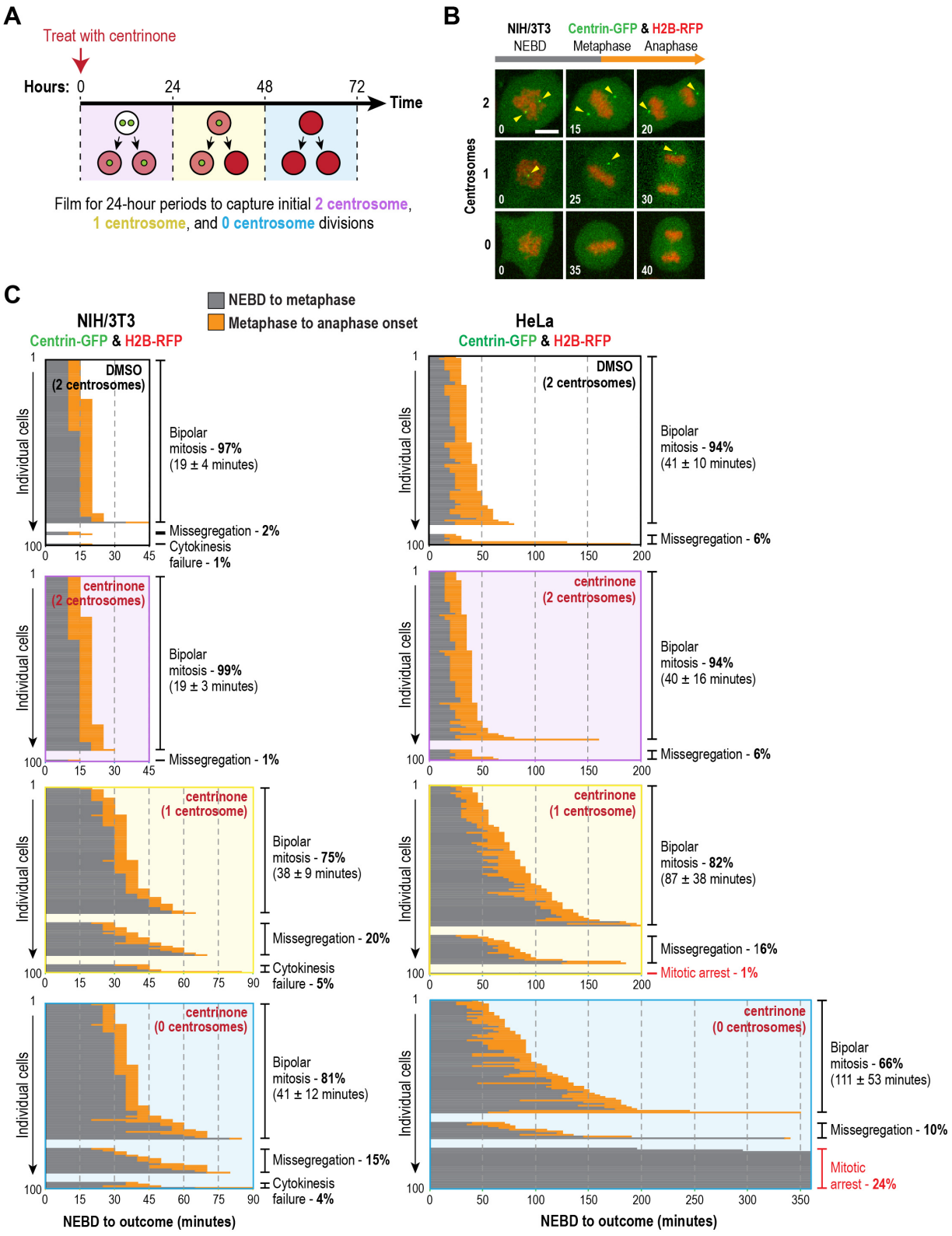
A
Treat with centrinone
Hours: 0 24 48 72 Time
Film for 24-hour periods to capture initial 2 centrosome, 1 centrosome, and 0 centrosome divisions
B
NIH/3T3
Centrin-GFP & H2B-RFP
NEBD
Metaphase
Anaphase
Centrosomes
2
1
0
C
NEBD to metaphase
Metaphase to anaphase onset
NIH/3T3
Centrin-GFP & H2B-RFP
HeLa
Centrin-GFP & H2B-RFP
Individual cells
DMSO (2 centrosomes)
Bipolar mitosis - 97% (19 ± 4 minutes)
Missegregation - 2%
Cytokinesis failure - 1%
centrinone (2 centrosomes)
Bipolar mitosis - 99% (19 ± 3 minutes)
Missegregation - 1%
centrinone (1 centrosome)
Bipolar mitosis - 75% (38 ± 9 minutes)
Missegregation - 20%
Cytokinesis failure - 5%
centrinone (0 centrosomes)
Bipolar mitosis - 81% (41 ± 12 minutes)
Missegregation - 15%
Cytokinesis failure - 4%
NEBD to outcome (minutes)
DMSO (2 centrosomes)
Bipolar mitosis - 94% (41 ± 10 minutes)
Missegregation - 6%
centrinone (2 centrosomes)
Bipolar mitosis - 94% (40 ± 16 minutes)
Missegregation - 6%
centrinone (1 centrosome)
Bipolar mitosis - 82% (87 ± 38 minutes)
Missegregation - 16%
Mitotic arrest - 1%
centrinone (0 centrosomes)
Bipolar mitosis - 66% (111 ± 53 minutes)
Missegregation - 10%
Mitotic arrest - 24%
NEBD to outcome (minutes)

Figure S7. Centrosome loss slows spindle assembly and leads to mitotic errors

(**A**) Schematic of the staggered treatment regime used to capture pioneer 2-, 1- and 0-centrosome mitoses. (**B**) Representative confocal images (maximum intensity projections) of 2-, 1- and 0-centrosome mitosis in NIH/3T3 cells co-expressing centrin-GFP and H2B-RFP. Yellow arrowheads indicate centrin foci. Times in the bottom left of each panel are in minutes relative to NEBD. Scale bar, 10 μm. (**C**) Plots of mitotic duration for NIH/3T3 and HeLa cells expressing centrin-GFP and H2B-RFP. Horizontal bars represent measurements from individual cells, ordered by the duration of NEBD to anaphase onset (*N*=2). Specific mitotic outcomes and associated percentages are indicated to the right of each box. Times in brackets are mean +/- SD of NEBD to anaphase onset. As centrosomes were lost, NIH/3T3 cells exhibited increases in chromosome missegregation and cytokinesis failure, and HeLa cells exhibited increases in chromosome missegregation and mitotic arrest, likely due to cohesion fatigue (*57*). These errors lead to cell death in mitosis or via apoptosis in the ensuing G1 (see **Fig. 2F** and **Fig. S6D**).

Wong et al. Figure S8

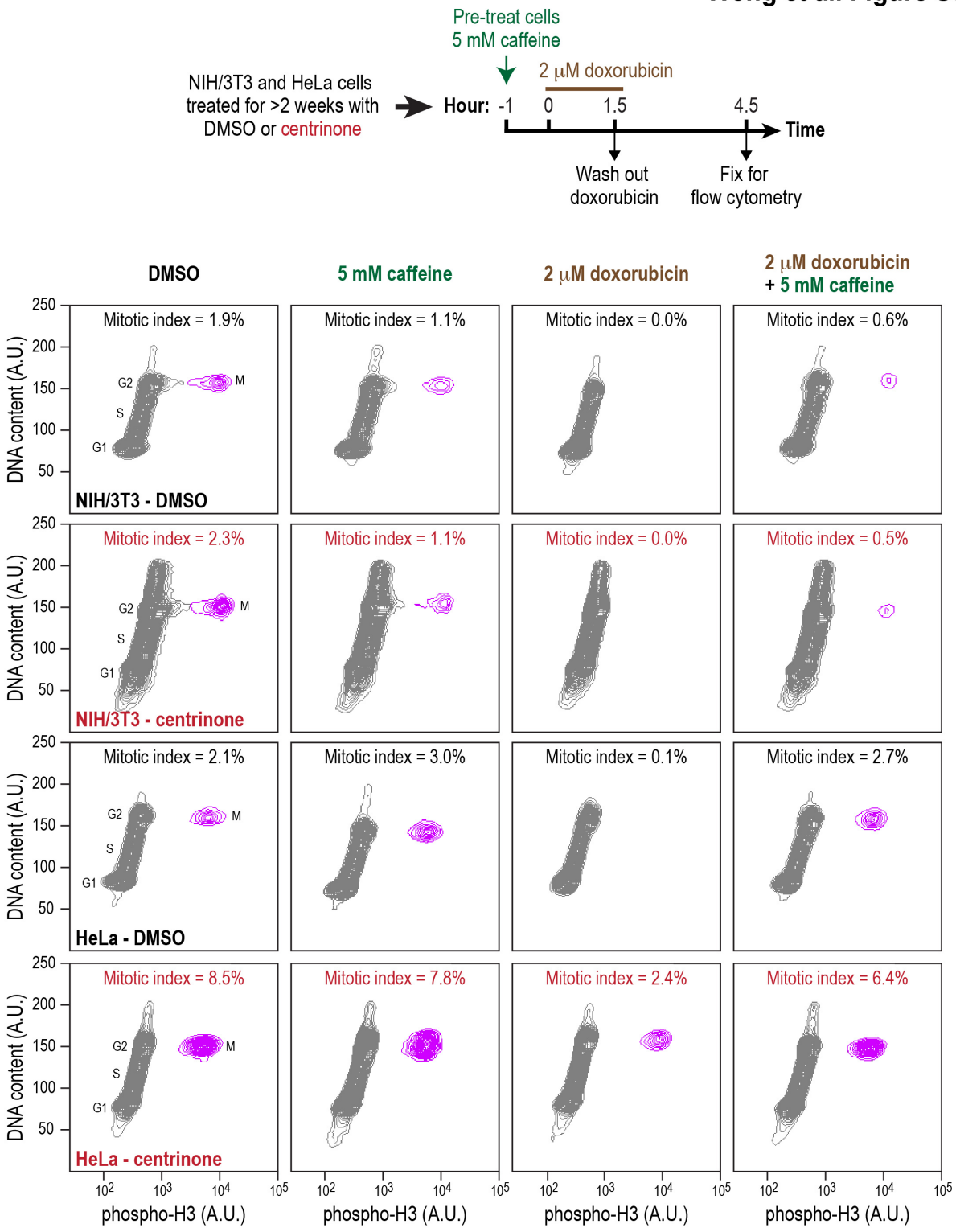

Figure S8. Cells maintain an intact DNA damage response in the absence of centrosomes

NIH/3T3 and HeLa cells were subjected to the schematized experimental protocol. Double-stranded DNA breaks were induced by treatment of cells with doxorubicin. DNA content analysis was used to measure the proportion of cells in mitosis, based on phospho-H3(S10) staining. In the presence of an intact G2 DNA damage checkpoint, the mitotic index of the population is reduced because cells that would have entered mitosis are arrested prior to mitotic entry, whereas cells already in mitosis can exit. Treatment of cells with 5 mM caffeine was used as a positive control for bypass of the DNA damage checkpoint. The mitotic index of centrinone-treated HeLa cells does not fall completely to zero after being challenged with doxorubicin because 24% of centrosome-less HeLa cells undergo a persistent mitotic arrest (see **Fig. S7**).

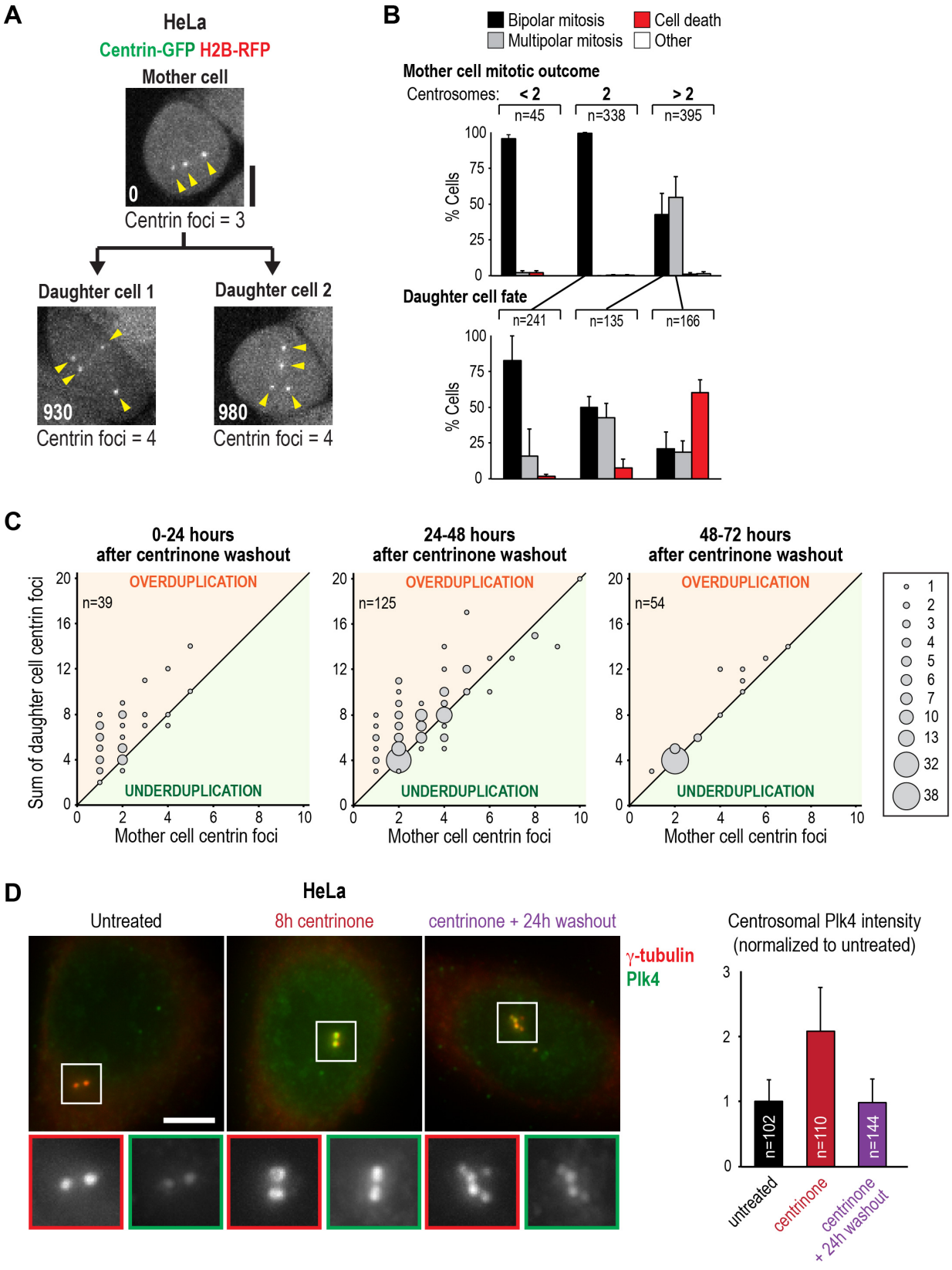
A
HeLa
Centrin-GFP H2B-RFP
Mother cell
0
Centrin foci = 3
Daughter cell 1
Daughter cell 2
930
980
Centrin foci = 4
Centrin foci = 4
B
Bipolar mitosis
Cell death
Multipolar mitosis
Other
Mother cell mitotic outcome
Centrosomes: < 2 2 > 2
n=45 n=338 n=395
% Cells
Daughter cell fate
n=241 n=135 n=166
C
0-24 hours after centrinone washout
24-48 hours after centrinone washout
48-72 hours after centrinone washout
OVERDUPLICATION
UNDERDUPLICATION
n=39
n=125
n=54
Sum of daughter cell centrin foci
Mother cell centrin foci
D
HeLa
Untreated
8h centrinone
centrinone + 24h washout
γ-tubulin
Plk4
Centrosomal Plk4 intensity
(normalized to untreated)
n=102
n=110
n=144
untreated
centrinone
centrinone + 24h washout

Figure S9. Centriole number set points arise from a dynamic equilibrium between centriole overduplication and removal of cells with extra centrioles

(**A**) Representative confocal images (maximum intensity projections) from a centrinone washout experiment in HeLa cells co-expressing centrin-GFP and H2B-RFP; only the GFP channel is shown. Yellow arrowheads mark centrin foci. Each frame was acquired at NEBD when the centrosomes are optimally distributed for counting. Times in the bottom left of each panel are in minutes relative to NEBD in the mother cell. Scale bar, 10 μm. (**B**) Histogram of mitotic outcomes for HeLa cells with <2, 2 or >2 centrosomes. The fates of daughter cells arising from 2-centrosome bipolar mitosis, multi-centrosome bipolar mitosis, and multi-centrosome multipolar mitosis are shown below. Data are mean +/- SD (*N*=2). (**C**) Plots of the number of centrin foci in the mother cell (x-axis) versus the sum of the centrin foci in her two daughter cells (y-axis) are shown for 3 different time intervals after centrinone washout (*N*=2). Intervals are based on the time of NEBD in the mother cells. The diagonal line represents the 2:1 ratio expected under normal conditions; points above or below this line correspond to over- or under-duplication, respectively. (**D**) Representative images of HeLa cells that were untreated, treated with 125 nM centrinone for 8 hours, or treated with centrinone for 8 hours followed by a 24-hour washout. Boxed regions are magnified 2.3X in panels below. Scale bar, 5 μm. The Plk4 intensity at centrosomes was quantified and normalized to the intensity in untreated cells. Data are mean +/- SD (*N*=3). An 8-hour centrinone treatment was sufficient to double the measured levels of Plk4 at the centrosome.

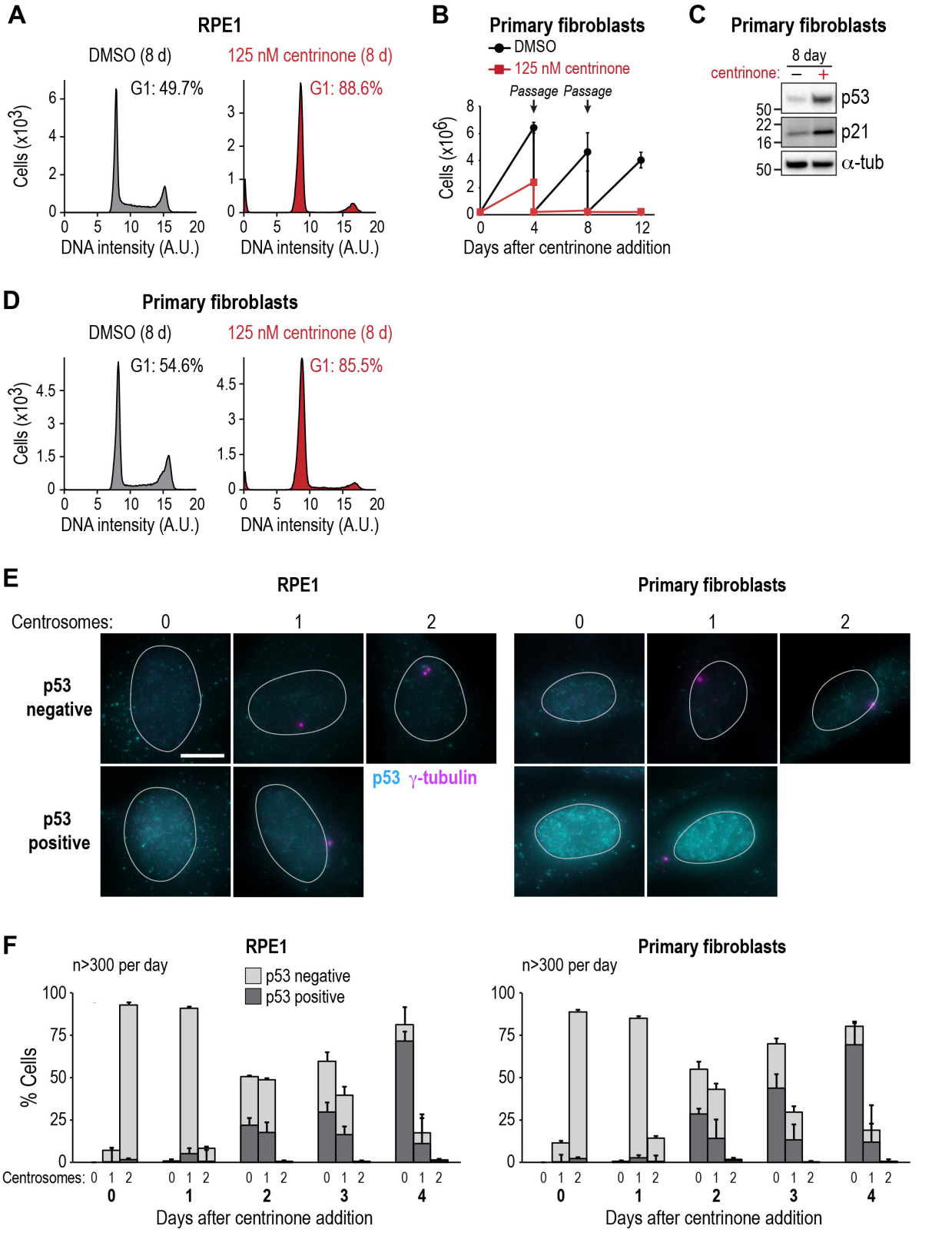
A
RPE1
DMSO (8 d)
125 nM centrinone (8 d)
G1: 49.7%
G1: 88.6%
Cells (x10^3)
DNA intensity (A.U.)
B
Primary fibroblasts
DMSO
125 nM centrinone
Passage Passage
Cells (x10^6)
Days after centrinone addition
C
Primary fibroblasts
8 day
centrinone: – +
p53
p21
α-tub
50
22
16
50
D
Primary fibroblasts
DMSO (8 d)
125 nM centrinone (8 d)
G1: 54.6%
G1: 85.5%
Cells (x10^3)
DNA intensity (A.U.)
E
RPE1
Primary fibroblasts
Centrosomes: 0 1 2
p53 negative
p53 positive
p53 γ-tubulin
F
RPE1
Primary fibroblasts
n>300 per day
p53 negative
p53 positive
% Cells
Centrosomes: 0 1 2
0 1 2 3 4
Days after centrinone addition

Figure S10. Centrosome loss triggers a p53-dependent arrest in normal cells within two to three cell cycles

(**A**) DNA content analysis of DMSO- and centrinone-treated RPE1 cells. The percentage of cells in G1 is indicated. (**B**) Passaging assay showing growth of primary fibroblasts immediately following addition of centrinone or DMSO as a control. Data are mean +/- SD (*N*=2). (**C**) Western Blot of p53 and p21 in primary fibroblasts after treatment with DMSO or centrinone for 8 days. (**D**) DNA content analysis of DMSO- and centrinone-treated primary fibroblasts. The percentage of cells in G1 is indicated. (**E**) Wide-field images of RPE1 cells and primary fibroblasts treated with centrinone for 1-3 days. Maximum intensity projections are shown. Nuclear boundaries are outlined in gray. A fraction of 1- and 0-centrosome cells exhibit increased nuclear p53 staining. Scale bar, 10 μm. (**F**) Quantification of p53-positive cells following centrinone addition to RPE1 and primary fibroblasts. Data are mean +/- SD (*N*=3).

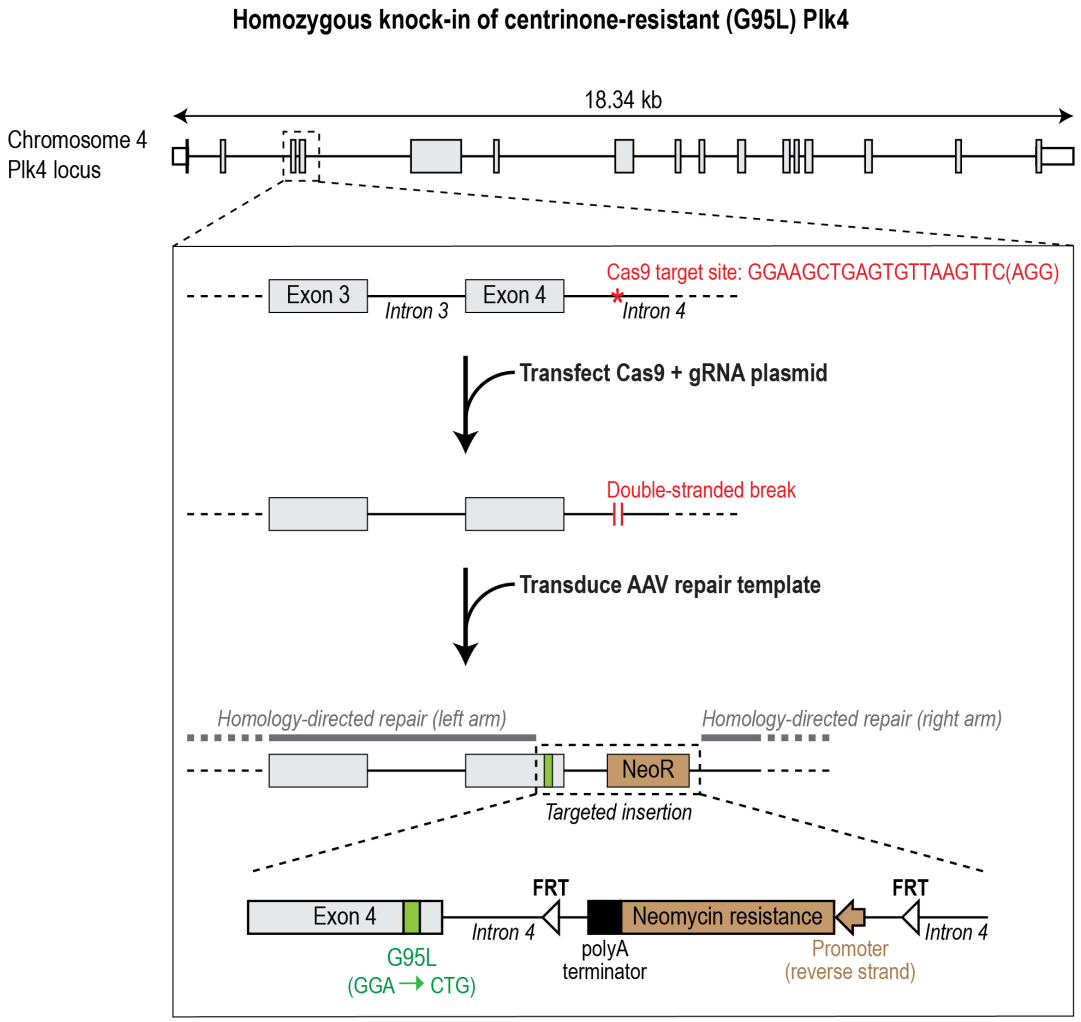

Figure S11. Generation of RPE1 cells with a centrinone-resistant (G95L) Plk4 knock-in

The codon for residue G95 is located in exon 4 of the Plk4 locus. A Cas9 recognition site within the intronic region between exons 4 and 5 was targeted to generate a double-stranded DNA break. AAV-mediated homology-directed repair was used to introduce the G95L point mutation into exon 4, together with a neomycin resistance cassette in the intron. The resistance cassette, driven by its own promoter on the anti-sense strand, enabled selection of clones positive for the knock-in. Homozygosity of the point mutation was verified by PCR and sequencing of genomic DNA at the locus.

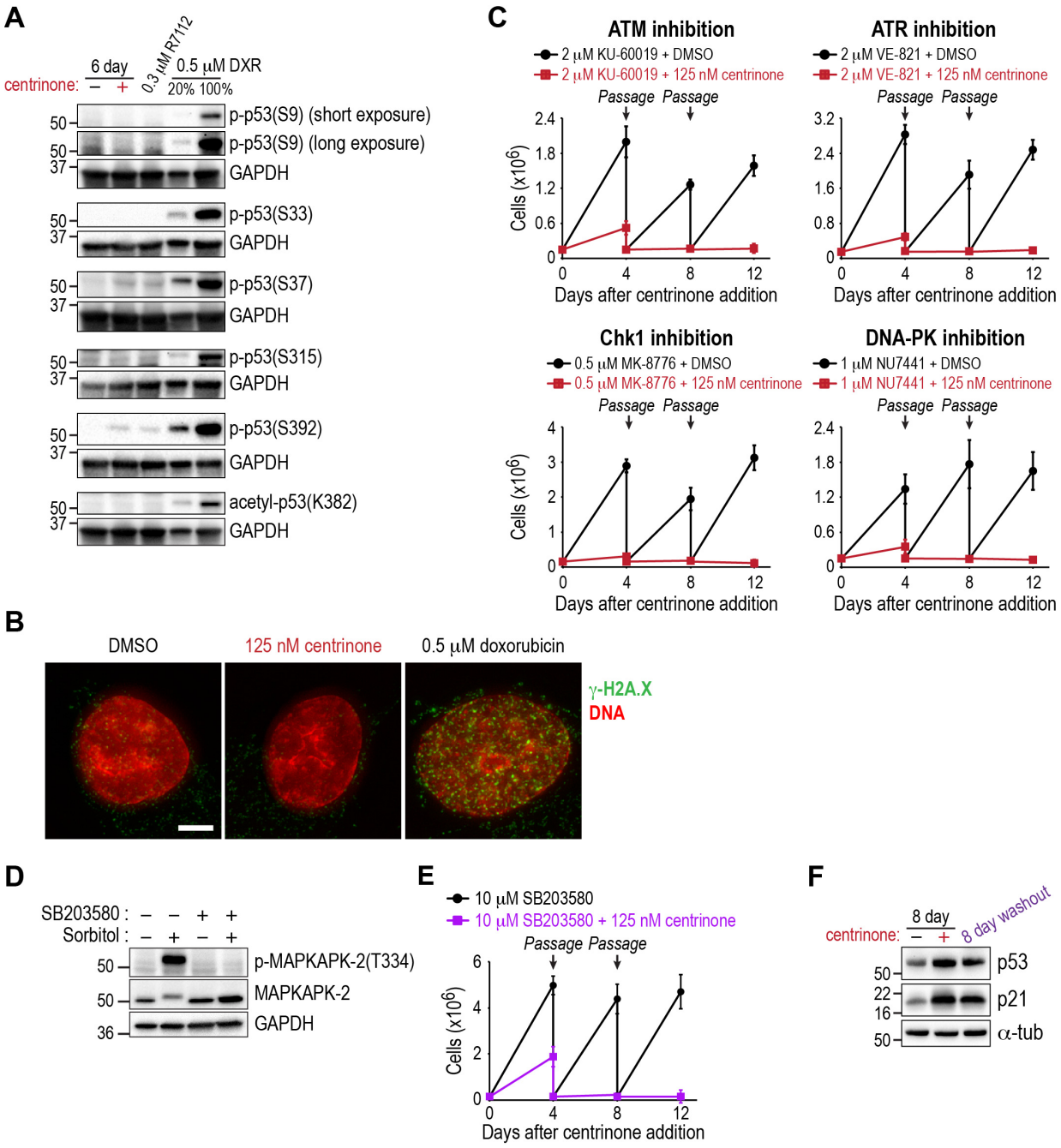
A
6 day
centrinone: – +
0.3 μM R7112
0.5 μM DXR
20% 100%
p-p53(S9) (short exposure)
p-p53(S9) (long exposure)
GAPDH
p-p53(S33)
GAPDH
p-p53(S37)
GAPDH
p-p53(S315)
GAPDH
p-p53(S392)
GAPDH
acetyl-p53(K382)
GAPDH
C
ATM inhibition
2 μM KU-60019 + DMSO
2 μM KU-60019 + 125 nM centrinone
ATR inhibition
2 μM VE-821 + DMSO
2 μM VE-821 + 125 nM centrinone
Chk1 inhibition
0.5 μM MK-8776 + DMSO
0.5 μM MK-8776 + 125 nM centrinone
DNA-PK inhibition
1 μM NU7441 + DMSO
1 μM NU7441 + 125 nM centrinone
Passage
Cells (x10^6)
Days after centrinone addition
B
DMSO
125 nM centrinone
0.5 μM doxorubicin
γ-H2A.X
DNA
D
SB203580 :
Sorbitol :
p-MAPKAPK-2(T334)
MAPKAPK-2
GAPDH
E
10 μM SB203580
10 μM SB203580 + 125 nM centrinone
F
8 day
8 day washout
centrinone:
p53
p21
α-tub

Figure S12. Arrest after centrosome loss is not related to DNA damage or stress

(**A**) Western Blot of p53 post-translational modifications from RPE1 cells treated with the indicated compounds. Ser9, Ser33, Ser37, Ser315 and Ser392 have been demonstrated to be phosphorylated in response to DNA damage (*58-62*), which also triggers acetylation of Lys382 (*57*). A 16-hour treatment with 0.5 μM doxorubicin was used as a positive control for induction of DNA damage. (**B**) Deconvolved wide-field images of γ-H2A.X foci in RPE1 cells treated with DMSO or centrinone for 4 days, or 0.5 μM doxorubicin as a control. The presence or absence (centrinone) of centrosomes in imaged cells was confirmed by γ-tubulin staining. Scale bar, 5 μm. (**C**) Passaging assays of RPE1 cells treated with the indicated inhibitors of the DNA damage response pathway, beginning immediately after centrinone addition. Data are mean +/- SD (*N*=2). (**D**) Western Blot of phospho-MAPKAPK-2 after induction of osmotic stress, in the presence or absence of the p38 MAPK inhibitor SB203580. SB203580 blocks phosphorylation of MAPKAPK-2 by p38. (**E**) Passaging assay of RPE1 cells treated with the p38 inhibitor SB203580, beginning immediately after centrinone addition. Data are mean +/- SD (*N*=2). (**F**) Western Blot of p53 and p21 in RPE1 cells treated with DMSO or centrinone for 8 days, or treated with centrinone for 8 days and then washed out for another 8 days. p53 and p21 levels remain elevated after centrinone washout.

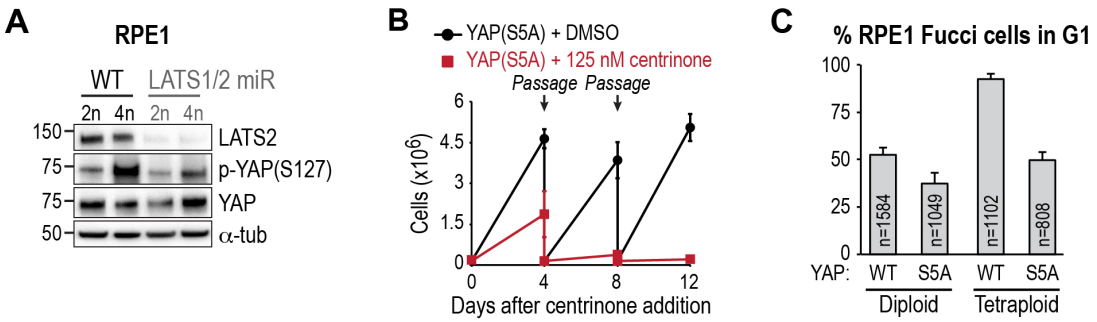

Figure S13. Arrest after centrosome loss is not related to the Hippo signaling pathway

Cytokinesis failure has been shown to trigger activation of the Hippo signaling pathway and subsequent cell cycle arrest (*27*). A key step in the activation of Hippo signaling is phosphorylation of YAP by LATS2 kinase. (**A**) Western Blot of LATS2, YAP and phospho-YAP(Ser127) in diploid and tetraploid RPE1 cells. Knockdown of LATS2 results in decreased YAP phosphorylation, even in tetraploid (4n) cells generated by induction of cytokinesis failure. (**B**) Passaging assay of RPE1 cells expressing constitutively-active (S5A) YAP that cannot be phosphorylated by LATS2, following addition of centrinone. Data are mean +/- SD (*N*=2). (**C**) Quantification of the percentage of YAP-expressing RPE1 Fucci cells in G1, 12 hours after drug washout. Diploid cells measurements were obtained from cells treated with DMSO for 24 hours before washout, whereas tetraploid cell measurements were obtained from cells treated with 4 μM cytochalasin D (to induce cytokinesis failure) for 24 hours before washout. Tetraploid cells expressing wild-type YAP are arrested at G1, whereas cells expressing constitutively-active (S5A) YAP bypass the arrest. Data are mean +/- SD (*N*=3).

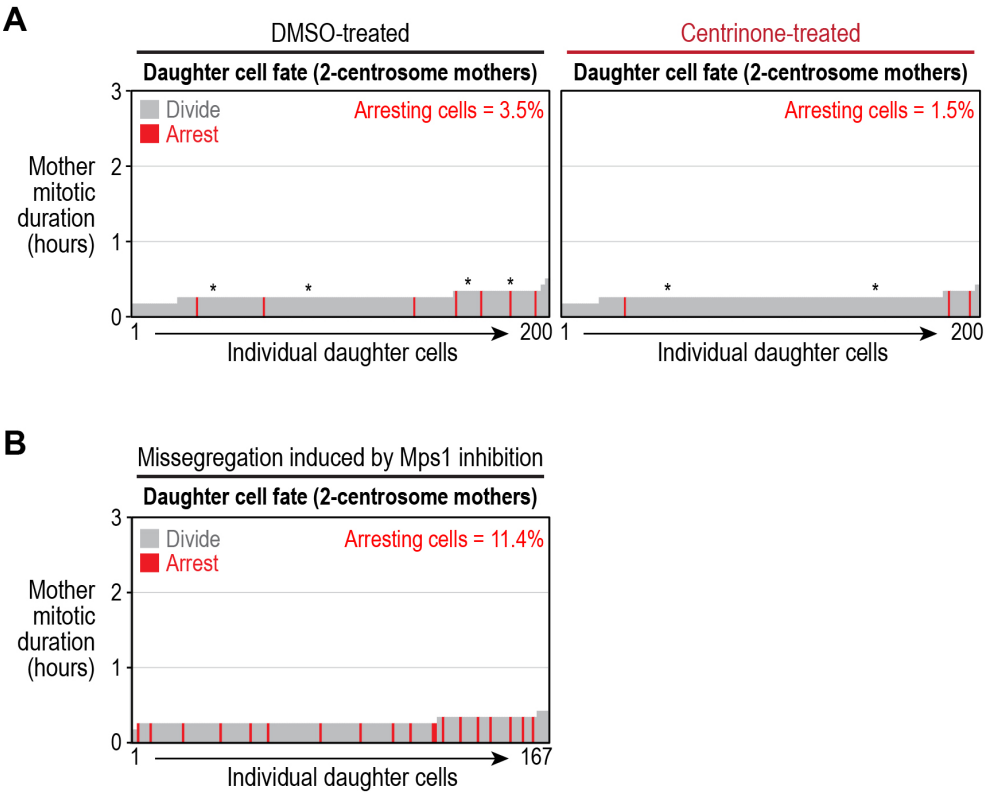

Figure S14. Arrest after centrosome loss is not related to the mitotic duration sensor or chromosome missegregation

Analysis of daughter cell fate in RPE1 cells expressing centrin-GFP and H2B-RFP. Vertical bars represent measurements from individual daughter cells (*N*=2). The height of each bar is the time their mother spent in prometaphase. (**A**) Cells treated with DMSO or centrinone. Asterisks (*) mark cases in which the mother cell had visible chromosome missegregation. The percentage of daughters not dividing within 48 hours = 3.5% (DMSO) and 1.5% (centrinone). (**B**) Cells treated with the Mps1 inhibitor NMS-P715. Only mitotic events with clear missegregation (lagging chromosomes and subsequent formation of daughter cells with micronuclei) were analyzed. The percentage of daughters not dividing within 48 hours = 11.4%.

Table S1. Data collection and refinement statistics.

Data collection	**Centrinone/Plk4 kinase domain**
Resolution (Å)	62.9 – 2.65
Space Group	I23
Unit Cell Dimensions (a, b, c) Å	125.8, 125.8, 125.8
Unit cell Angles (α,β,γ) °	90, 90, 90
I/σ (last shell)	30.4 (1.7)
[a]R_{sym} (last shell)	0.102 (2.423)
[b]R_{meas} (last shell)	0.104 (2.478)
[c]$CC_{1/2}$ (last shell)	1.000 (0.632)
Completeness (last shell) %	100.0 (100.0)
Number of reflections	217426
Unique	9793
Multiplicity (last shell)	22.2 (22.5)
Refinement	
Resolution (Å)	62.9 – 2.65 (3.04-2.65)
Number of reflections	
Working	9313
Free	469
[d]R_{work} (last shell) (%)	19.92 (25.26)
[d]R_{free} (last shell) (%)	26.95 (36.54)
Structure/Stereochemistry	
Number of atoms	1750
Solvent	43
Ligand	12
r.m.s.d. bond lengths (Å)	0.008
r.m.s.d. bond angles (°)	1.389
Average B-Factor	47.07
Protein Data Bank ID[e]	4YUR

[a]$R_{sym} = \sum\sum j|I_j - \langle I\rangle|/\sum I_j$, where I_j is the intensity measurement for reflection j and $\langle I\rangle$ is the mean intensity for multiply recorded reflections.

[b]$R_{meas} = \sum_h [\sqrt{(n/(n-1))}\ \sum_j [I_{hj} - \langle I_h\rangle] / \sum_{hj} \langle I_h\rangle$, where I_{hj} is a single intensity measurement for reflection h, $\langle I_h\rangle$ is the average intensity measurement for multiply recorded reflections, and n is the number of observations of reflection h.

[c]$CC_{1/2}$ is the Pearson correlation coefficient between the average measured intensities of two randomly-assigned half-sets of the measurements of each unique reflection (*63*). $CC_{1/2}$ is considered significant above a value of ~0.15.

[d]$R_{work,\ free} = \sum||F_{obs}| - |F_{calc}||/|F_{obs}|$, where the working and free *R*-factors are calculated using the working and free reflection sets, respectively.

[e]Coordinates and structure factors have been deposited with the Protein Data Bank (http://www.pdb.org) with the noted accession code.

Table S2. K_i values and selectivities of centrinone, centrinone-B and VX-680 for the inhibitor-resistant mutant Plk4 (G95L) and Aurora A/B. Selectivity is defined as K_i(kinase)/K_i(Plk4). Dash, N.A.

Kinase	K_i (nM)			Plk4 selectivity		
	Centrinone	Centrinone-B	VX-680	Centrinone	Centrinone-B	VX-680
Plk4	**0.16**	**0.59**	**7.66**	**-**	**-**	**-**
Plk4 (G95L)	68.57	497.53	9291.67	432	847	1213
Aurora A	171.00	1239.00	0.65	1078	2108	0.08
Aurora B	436.76	5597.14	3.36	2754	9523	0.44

Table S3. DiscoveRx KINOMEscan profiling of centrinone (100 nM) and centrinone-B (300 nM) against 442 human kinases. As an Excel file.

K_i values were determined for the 8 wild-type kinases (including Plk4) where signal was <35% of control (>65% probe displacement) as well as Aurora A and B (bold) (see Tables S2 and S4).

Table S4. K_i values and selectivities of centrinone and centrinone-B for the top 7 identified off-targets from DiscoveRx kinome profiling. Selectivity is defined as K_i(kinase)/K_i(Plk4). Dash, N.A.

Kinase	K_i (nM)		Plk4 selectivity	
	Centrinone	Centrinone-B	Centrinone	Centrinone-B
Plk4	**0.16**	**0.59**	**-**	**-**
TNK1	1.38	6.04	9	10
LRRK2	2.08	7.66	13	13
ROS/ROS1	2.77	90.07	18	153
FLT4/VEGFR3	6.29	58.04	40	99
RET	13.92	195.25	88	332
JAK2	>150	>500	>938	>847
SRPK1	>150	>500	>938	>847

Table S5. Cell lines that proliferate in the absence of centrosomes.

Cell lines are ordered by the degree of centrosome amplification (percentage of cells with >2 γ-tubulin/Cep192 foci) in untreated cells.

CELL LINE	ORIGIN	CENTROSOME AMPLIFICATION (%)	p53 and CDKN2A STATUS
CT26.WT[a]	Colon carcinoma	2	CDKN2A deleted
U-138 MG	Glioblastoma	3	p53 mutated
HeLa	Cervical carcinoma	4	p53 degraded (HPV)
Ca Ski	Cervical carcinoma	4	p53 degraded (HPV)
SW837	Rectal carcinoma	4	p53 mutated
DLD-1	Colon carcinoma	5	p53 mutated
NCI-H358	Lung carcinoma	5	p53 mutated
SJSA-1	Osteosarcoma	5	p53 degraded (MDM2 amplification)
MCF 10A	Breast epithelial	5	CDKN2A deleted
LNCaP	Prostate carcinoma	5	Wild-type
NIH/3T3[a]	Embryonic fibroblast	6	CDKN2A deleted
C-33 A	Cervical carcinoma	6	p53 mutated
LOX IMVI	Melanoma	6	CDKN2A deleted
U2OS	Osteosarcoma	7	CDKN2A silenced
HCT116	Colon carcinoma	9	CDKN2A silenced
Calu-6	Lung carcinoma	11	p53 mutated
MDA-MB-231	Breast carcinoma	16	p53 mutated
BT-549	Breast carcinoma	19	p53 mutated
RD	Rhabdomyosarcoma	22	p53 mutated
B16-F10[a]	Melanoma	27	CDKN2A deleted
N1E-115-1[a]	Neuroblastoma	81	Not known

[a]Mouse cell line

Table S6. Cell lines and primary cell cultures that arrest in response to centrosome depletion. Cell lines are ordered by the degree of centrosome amplification (percentage of cells with >2 γ-tubulin/Cep192 foci) in untreated cells.

CELL LINE	ORIGIN	CENTROSOME AMPLIFICATION (%)	p53 STATUS
Primary dermal fibroblast		0	Wild-type
Primary umbilical vein endothelial		0	Wild-type
Primary mammary epithelial		0	Wild-type
BJ-5ta	Foreskin fibroblast	0	Wild-type
RPE1	Retinal pigment epithelial	1	Wild-type
IMR-90	Lung fibroblast	3	Wild-type

REFERENCES AND NOTES

1. I. A. Drummond, Cilia functions in development. *Curr. Opin. Cell Biol.* **24**, 24–30 (2012). Medline doi:10.1016/j.ceb.2011.12.007

2. H. Schatten, The mammalian centrosome and its functional significance. *Histochem. Cell Biol.* **129**, 667–686 (2008). Medline doi:10.1007/s00418-008-0427-6

3. D. A. Brito, S. M. Gouveia, M. Bettencourt-Dias, Deconstructing the centriole: Structure and number control. *Curr. Opin. Cell Biol.* **24**, 4–13 (2012). Medline doi:10.1016/j.ceb.2012.01.003

4. E. N. Färat-Karalar, T. Stearns, The centriole duplication cycle. *Philos. Trans. R. Soc. Lond. B Biol. Sci.* **369**, 20130460 (2014). Medline doi:10.1098/rstb.2013.0460

5. T. Boveri, *Zur Frage der Entstehung maligner Tumoren* (Gustav Fischer, Jena, 1914).

6. S. A. Godinho, D. Pellman, Causes and consequences of centrosome abnormalities in cancer. *Philos. Trans. R. Soc. Lond. B Biol. Sci.* **369**, 20130467 (2014). Medline

7. E. A. Nigg, L. Čajánek, C. Arquint, The centrosome duplication cycle in health and disease. *FEBS Lett.* **588**, 2366–2372 (2014). Medline doi:10.1016/j.febslet.2014.06.030

8. N. J. Ganem, S. A. Godinho, D. Pellman, A mechanism linking extra centrosomes to chromosomal instability. *Nature* **460**, 278–282 (2009). Medline doi:10.1038/nature08136

9. W. T. Silkworth, I. K. Nardi, L. M. Scholl, D. Cimini, Multipolar spindle pole coalescence is a major source of kinetochore mis-attachment and chromosome mis-segregation in cancer cells. *PLOS ONE* **4**, e6564 (2009). Medline doi:10.1371/journal.pone.0006564

10. S. A. Godinho, R. Picone, M. Burute, R. Dagher, Y. Su, C. T. Leung, K. Polyak, J. S. Brugge, M. Théry, D. Pellman, Oncogene-like induction of cellular invasion from centrosome amplification. *Nature* **510**, 167–171 (2014). Medline doi:10.1038/nature13277

11. M. Bettencourt-Dias, A. Rodrigues-Martins, L. Carpenter, M. Riparbelli, L. Lehmann, M. K. Gatt, N. Carmo, F. Balloux, G. Callaini, D. M. Glover, SAK/PLK4 is required for centriole duplication and flagella development. *Curr. Biol.* **15**, 2199–2207 (2005). Medline doi:10.1016/j.cub.2005.11.042

12. R. Habedanck, Y. D. Stierhof, C. J. Wilkinson, E. A. Nigg, The Polo kinase Plk4 functions in centriole duplication. *Nat. Cell Biol.* **7**, 1140–1146 (2005). Medline doi:10.1038/ncb1320

13. J. Kleylein-Sohn, J. Westendorf, M. Le Clech, R. Habedanck, Y. D. Stierhof, E. A. Nigg, Plk4-induced centriole biogenesis in human cells. *Dev. Cell* **13**, 190–202 (2007). Medline doi:10.1016/j.devcel.2007.07.002

14. K. F. O'Connell, C. Caron, K. R. Kopish, D. D. Hurd, K. J. Kemphues, Y. Li, J. G. White, The C. elegans zyg-1 gene encodes a regulator of centrosome duplication with distinct maternal and paternal roles in the embryo. *Cell* **105**, 547–558 (2001). Medline doi:10.1016/S0092-8674(01)00338-5

15. N. Peel, N. R. Stevens, R. Basto, J. W. Raff, Overexpressing centriole-replication proteins in vivo induces centriole overduplication and de novo formation. *Curr. Biol.* **17**, 834–843 (2007). Medline doi:10.1016/j.cub.2007.04.036

16. M. I. Davis, J. P. Hunt, S. Herrgard, P. Ciceri, L. M. Wodicka, G. Pallares, M. Hocker, D. K. Treiber, P. P. Zarrinkar, Comprehensive analysis of kinase inhibitor selectivity. *Nat. Biotechnol.* **29**, 1046–1051 (2011). Medline doi:10.1038/nbt.1990

17. E. F. Johnson, K. D. Stewart, K. W. Woods, V. L. Giranda, Y. Luo, Pharmacological and functional comparison of the polo-like kinase family: Insight into inhibitor and substrate specificity. *Biochemistry* **46**, 9551–9563 (2007). Medline doi:10.1021/bi7008745

18. J. M. Mason, D. C. Lin, X. Wei, Y. Che, Y. Yao, R. Kiarash, D. W. Cescon, G. C. Fletcher, D. E. Awrey, M. R. Bray, G. Pan, T. W. Mak, Functional characterization of CFI-400945, a Polo-like kinase 4 inhibitor, as a potential anticancer agent. *Cancer Cell* **26**, 163–176 (2014). Medline doi:10.1016/j.ccr.2014.05.006

19. P. B. Sampson, Y. Liu, B. Forrest, G. Cumming, S. W. Li, N. K. Patel, L. Edwards, R. Laufer, M. Feher, F. Ban, D. E. Awrey, G. Mao, O. Plotnikova, R. Hodgson, I. Beletskaya, J. M. Mason, X. Luo, V. Nadeem, X. Wei, R. Kiarash, B. Madeira, P. Huang, T. W. Mak, G. Pan, H. W. Pauls, The discovery of Polo-like kinase 4 inhibitors: Identification of (1R,2S).2-(3-((E).4-(((cis).2,6-dimethylmorpholino)methyl)styryl). 1H.indazol-6-yl)-5 methoxyspiro[cyclopropane-1,3 indolin]-2 one (CFI-400945) as a potent, orally active antitumor agent. *J. Med. Chem.* **58**, 147–169 (2015). Medline doi:10.1021/jm5005336

20. D. A. Sloane, M. Z. Trikic, M. L. Chu, M. B. Lamers, C. S. Mason, I. Mueller, W. J. Savory, D. H. Williams, P. A. Eyers, Drug-resistant aurora A mutants for cellular target validation of the small molecule kinase inhibitors MLN8054 and MLN8237. *ACS Chem. Biol.* **5**, 563–576 (2010). Medline doi:10.1021/cb100053q

21. R. M. Rios, The centrosome-Golgi apparatus nexus. *Philos. Trans. R. Soc. Lond. B Biol. Sci.* **369**, 20130462 (2014). Medline doi:10.1098/rstb.2013.0462

22. A. Khodjakov, C. L. Rieder, Centrosomes enhance the fidelity of cytokinesis in vertebrates and are required for cell cycle progression. *J. Cell Biol.* **153**, 237–242 (2001). Medline doi:10.1083/jcb.153.1.237

23. J. H. Sir, M. Pütz, O. Daly, C. G. Morrison, M. Dunning, J. V. Kilmartin, F. Gergely, Loss of centrioles causes chromosomal instability in vertebrate somatic cells. *J. Cell Biol.* **203**, 747–756 (2013). Medline doi:10.1083/jcb.201309038

24. Y. Uetake, J. Loncarek, J. J. Nordberg, C. N. English, S. La Terra, A. Khodjakov, G. Sluder, Cell cycle progression and de novo centriole assembly after centrosomal removal in untransformed human cells. *J. Cell Biol.* **176**, 173–182 (2007). Medline doi:10.1083/jcb.200607073

25. L. M. Jenkins, S. R. Durell, S. J. Mazur, E. Appella, p53 N-terminal phosphorylation: A defining layer of complex regulation. *Carcinogenesis* **33**, 1441–1449 (2012). Medline doi:10.1093/carcin/bgs145

26. N. D. Lakin, S. P. Jackson, Regulation of p53 in response to DNA damage. *Oncogene* **18**, 7644–7655 (1999). Medline doi:10.1038/sj.onc.1203015

27. N. J. Ganem, H. Cornils, S. Y. Chiu, K. P. O'Rourke, J. Arnaud, D. Yimlamai, M. Théry, F. D. Camargo, D. Pellman, Cytokinesis failure triggers hippo tumor suppressor pathway activation. *Cell* **158**, 833–848 (2014). Medline doi:10.1016/j.cell.2014.06.029

28. Y. Uetake, G. Sluder, Prolonged prometaphase blocks daughter cell proliferation despite normal completion of mitosis. *Curr. Biol.* **20**, 1666–1671 (2010). Medline doi:10.1016/j.cub.2010.08.018

29. H. Bazzi, K. V. Anderson, Acentriolar mitosis activates a p53-dependent apoptosis pathway in the mouse embryo. *Proc. Natl. Acad. Sci. U.S.A.* **111**, E1491–E1500 (2014). Medline doi:10.1073/pnas.1400568111

30. D. Izquierdo, W. J. Wang, K. Uryu, M. F. Tsou, Stabilization of cartwheel-less centrioles for duplication requires CEP295-mediated centriole-to-centrosome conversion. *Cell Reports* **8**, 957–965 (2014). Medline doi:10.1016/j.celrep.2014.07.022

31. H. Shen, C. G. Maki, Pharmacologic activation of p53 by small-molecule MDM2 antagonists. *Curr. Pharm. Des.* **17**, 560–568 (2011). Medline doi:10.2174/138161211795222603

32. R. Basto, J. Lau, T. Vinogradova, A. Gardiol, C. G. Woods, A. Khodjakov, J. W. Raff, Flies without centrioles. *Cell* **125**, 1375–1386 (2006). Medline doi:10.1016/j.cell.2006.05.025

33. F. Bartolini, G. G. Gundersen, Generation of noncentrosomal microtubule arrays. *J. Cell Sci.* **119**, 4155–4163 (2006). Medline doi:10.1242/jcs.03227

34. M. Stiess, N. Maghelli, L. C. Kapitein, S. Gomis-Rüth, M. Wilsch-Bräuninger, C. C. Hoogenraad, I. M. Tolić-Nørrelykke, F. Bradke, Axon extension occurs independently of centrosomal microtubule nucleation. *Science* **327**, 704–707 (2010). Medline doi:10.1126/science.1182179

35. K. D. Sumigray, T. Lechler, Control of cortical microtubule organization and desmosome stability by centrosomal proteins. *BioArchitecture* **1**, 221–224 (2011). Medline doi:10.4161/bioa.18403

36. E. Harlow, D. Lane, *Antibodies: A Laboratory Manual* (Cold Spring Harbor Laboratory Press, Cold Spring Harbor, NY, 1988).

37. Y.-C. Cheng, W. H. Prusoff, Relationship between the inhibition constant (K1) and the concentration of inhibitor which causes 50 per cent inhibition (I50) of an enzymatic reaction. *Biochem. Pharmacol.* **22**, 3099–3108 (1973). Medline doi:10.1016/0006-2952(73)90196-2

38. R. A. Copeland, J. P. Davis, R. L. Dowling, D. Lombardo, K. B. Murphy, T. A. Patterson, Recombinant human dihydroorotate dehydrogenase: Expression, purification, and characterization of a catalytically functional truncated enzyme. *Arch. Biochem. Biophys.* **323**, 79–86 (1995). Medline doi:10.1006/abbi.1995.0012

39. W. Kabsch, Xds. *Acta Crystallogr. D Biol. Crystallogr.* **66**, 125–132 (2010). Medline doi:10.1107/S0907444909047337

40. M. D. Winn, C. C. Ballard, K. D. Cowtan, E. J. Dodson, P. Emsley, P. R. Evans, R. M. Keegan, E. B. Krissinel, A. G. Leslie, A. McCoy, S. J. McNicholas, G. N. Murshudov, N. S. Pannu, E. A. Potterton, H. R. Powell, R. J. Read, A. Vagin, K. S. Wilson, Overview of the CCP4 suite and current developments. *Acta Crystallogr. D Biol. Crystallogr.* **67**, 235–242 (2011). Medline doi:10.1107/S0907444910045749

41. A. J. McCoy, R. W. Grosse-Kunstleve, P. D. Adams, M. D. Winn, L. C. Storoni, R. J. Read, Phaser crystallographic software. *J. Appl. Cryst.* **40**, 658–674 (2007). Medline doi:10.1107/S0021889807021206

42. P. D. Adams, P. V. Afonine, G. Bunkóczi, V. B. Chen, I. W. Davis, N. Echols, J. J. Headd, L. W. Hung, G. J. Kapral, R. W. Grosse-Kunstleve, A. J. McCoy, N. W. Moriarty, R. Oeffner, R. J. Read, D. C. Richardson, J. S. Richardson, T. C. Terwilliger, P. H. Zwart, PHENIX: A comprehensive Python-based system for macromolecular structure solution. *Acta Crystallogr. D Biol. Crystallogr.* **66**, 213–221 (2010). Medline doi:10.1107/S0907444909052925

43. K. Muller *et al*., MOLOC: A molecular modeling program. *Bull. Soc. Chim. Belg.* **97**, 655–667 (1988).

44. F. A. Ran, P. D. Hsu, J. Wright, V. Agarwala, D. A. Scott, F. Zhang, Genome engineering using the CRISPR-Cas9 system. *Nat. Protoc.* **8**, 2281–2308 (2013). Medline doi:10.1038/nprot.2013.143

45. E. Berdougo, M. E. Terret, P. V. Jallepalli, Functional dissection of mitotic regulators through gene targeting in human somatic cells. *Methods Mol. Biol.* **545**, 21–37 (2009). Medline doi:10.1007/978-1-60327-993-2_2

46. Z. Yang, K. Nakagawa, A. Sarkar, J. Maruyama, H. Iwasa, Y. Bao, M. Ishigami-Yuasa, S. Ito, H. Kagechika, S. Hata, H. Nishina, S. Abe, M. Kitagawa, Y. Hata, Screening with a novel cell-based assay for TAZ activators identifies a compound that enhances myogenesis in C2C12 cells and facilitates muscle repair in a muscle injury model. *Mol. Cell. Biol.* **34**, 1607–1621 (2014). Medline doi:10.1128/MCB.01346-13

47. S. Lawo, M. Hasegan, G. D. Gupta, L. Pelletier, Subdiffraction imaging of centrosomes reveals higher-order organizational features of pericentriolar material. *Nat. Cell Biol.* **14**, 1148–1158 (2012). Medline doi:10.1038/ncb2591

48. K. F. Sonnen, L. Schermelleh, H. Leonhardt, E. A. Nigg, 3D-structured illumination microscopy provides novel insight into architecture of human centrosomes. *Biol. Open* **1**, 965–976 (2012). Medline doi:10.1242/bio.20122337

49. H. L. Sive, R. M. Grainger, R. M. Harland, *Early Development of* Xenopus laevis: *A Laboratory Manual* (Cold Spring Harbor Laboratory Press, Cold Spring Harbor, NY, 2000).

50. J. L. Stubbs, E. K. Vladar, J. D. Axelrod, C. Kintner, Multicilin promotes centriole assembly and ciliogenesis during multiciliate cell differentiation. *Nat. Cell Biol.* **14**, 140–147 (2012). Medline doi:10.1038/ncb2406

51. D. A. Klos Dehring, E. K. Vladar, M. E. Werner, J. W. Mitchell, P. Hwang, B. J. Mitchell, Deuterosome-mediated centriole biogenesis. *Dev. Cell* **27**, 103–112 (2013). Medline doi:10.1016/j.devcel.2013.08.021

52. S. Zitouni, C. Nabais, S. C. Jana, A. Guerrero, M. Bettencourt-Dias, Polo-like kinases: Structural variations lead to multiple functions. *Nat. Rev. Mol. Cell Biol.* **15**, 433–452 (2014). Medline doi:10.1038/nrm3819

53. A. J. Holland, W. Lan, S. Niessen, H. Hoover, D. W. Cleveland, Polo-like kinase 4 kinase activity limits centrosome overduplication by autoregulating its own stability. *J. Cell Biol.* **188**, 191–198 (2010). Medline doi:10.1083/jcb.200911102

54. I. Akritopoulou-Zanze, P. J. Hajduk, Kinase-targeted libraries: The design and synthesis of novel, potent, and selective kinase inhibitors. *Drug Discov. Today* **14**, 291–297 (2009). Medline doi:10.1016/j.drudis.2008.12.002

55. M. Kothe, D. Kohls, S. Low, R. Coli, G. R. Rennie, F. Feru, C. Kuhn, Y. H. Ding, Selectivity-determining residues in Plk1. *Chem. Biol. Drug Des.* **70**, 540–546 (2007). Medline doi:10.1111/j.1747-0285.2007.00594.x

56. H. Leonhardt, H. P. Rahn, P. Weinzierl, A. Sporbert, T. Cremer, D. Zink, M. C. Cardoso, Dynamics of DNA replication factories in living cells. *J. Cell Biol.* **149**, 271–280 (2000). Medline doi:10.1083/jcb.149.2.271

57. G. J. Gorbsky, Cohesion fatigue. *Curr. Biol.* **23**, R986–R988 (2013). Medline doi:10.1016/j.cub.2013.08.017

58. Y. Higashimoto, S. Saito, X. H. Tong, A. Hong, K. Sakaguchi, E. Appella, C. W. Anderson, Human p53 is phosphorylated on serines 6 and 9 in response to DNA damage-inducing agents. *J. Biol. Chem.* **275**, 23199–23203 (2000). Medline doi:10.1074/jbc.M002674200

59. S. Y. Shieh, M. Ikeda, Y. Taya, C. Prives, DNA damage-induced phosphorylation of p53 alleviates inhibition by MDM2. *Cell* **91**, 325–334 (1997). Medline doi:10.1016/S0092-8674(00)80416-X

60. K. Sakaguchi, J. E. Herrera, S. Saito, T. Miki, M. Bustin, A. Vassilev, C. W. Anderson, E. Appella, DNA damage activates p53 through a phosphorylation-acetylation cascade. *Genes Dev.* **12**, 2831–2841 (1998). Medline doi:10.1101/gad.12.18.2831

61. J. P. Blaydes, M. G. Luciani, S. Pospisilova, H. M. Ball, B. Vojtesek, T. R. Hupp, Stoichiometric phosphorylation of human p53 at Ser315 stimulates p53-dependent transcription. *J. Biol. Chem.* **276**, 4699–4708 (2001). Medline doi:10.1074/jbc.M003485200

62. M. L. Cox, D. W. Meek, Phosphorylation of serine 392 in p53 is a common and integral event during p53 induction by diverse stimuli. *Cell. Signal.* **22**, 564–571 (2010). Medline doi:10.1016/j.cellsig.2009.11.014

63. P. A. Karplus, K. Diederichs, Linking crystallographic model and data quality. *Science* **336**, 1030–1033 (2012). Medline doi:10.1126/science.1218231